J. Fluid Mech. (1996), vol. 326, pp. 205–237
Copyright © 1996 Cambridge University Press

Effects of molecular diffusivities on counter-gradient scalar and momentum transfer in strongly stable stratification

By SATORU KOMORI AND KOUJI NAGATA

Department of Chemical Engineering, Kyushu University, Hakozaki, Fukuoka 812-81, Japan

(Received 16 January 1995 and in revised form 31 May 1996)

The effects of molecular diffusivities of heat and mass on the counter-gradient scalar and momentum transfer in strongly stable stratification are experimentally investigated in unsheared and sheared stratified water mixing-layer flows downstream of turbulence-generating grids. Experiments are carried out in two kinds of stably stratified water flows. In the case of thermal stratification, the difference between the turbulent fluxes of an active scalar (heat with the Prandtl number of $Pr \approx 6$) and a passive scalar (mass with the Schmidt number of $Sc \approx 600$) is investigated. In the case of salt stratification, the effects of the molecular diffusion of the active scalar (salt) with a very high Schmidt number of $Sc \approx 600$ on the counter-gradient scalar transfer is studied. Comparisons of the effects of molecular diffusivities are also made between thermally stratified water and air ($Pr \approx 0.7$) flows. Further, the effects of mean shear on the counter-gradient scalar and momentum transfer are investigated for both stratified cases. Instantaneous temperature, concentration and streamwise and vertical velocities are simultaneously measured using a combined technique with a resistance thermometer, a laser-induced fluorescence method, and a laser-Doppler velocimeter with high spatial resolution. Turbulent scalar fluxes, joint probability density functions, and cospectra are estimated.

The results of the first case show that both active heat and passive mass develop counter-gradient fluxes but that the counter-gradient flux of passive mass is about 10% larger than that of active heat, mostly due to molecular diffusion effects at small scales. The counter-gradient scalar transfer mechanism in stable stratification can be explained by considering the relative balance between the available potential energy and the turbulent kinetic energy as in Schumann (1987). In thermally and salt-stratified water mixing-layer flows with the active scalars of high Prandtl and Schmidt numbers, the buoyancy-induced motions with finger-like structures first contribute to the counter-gradient scalar fluxes at small scales, and then the large-scale motions, which bring fluid back to its original levels, generate the counter-gradient fluxes at large scales. The contribution of the small-scale motions to the counter-gradient fluxes in stratified water flows is quite different from that in stratified air flows. The higher Prandtl or Schmidt number of the active scalar generates both the stronger buoyancy effects and the longer time-oscillation period of the counter-gradient scalar fluxes. The time-oscillation occurs at large scales but the counter-gradient fluxes at small scales persist without oscillating. The mean shear acts to reduce the counter-gradient scalar and momentum transfer at large scales, and therefore the counter-gradient fluxes in sheared stratified flows can be seen only in very strong stratification. The behaviour of the counter-gradient mo-

mentum flux in strong stratification is quite similar to that of the counter-gradient scalar flux.

1. Introduction

Density-stratified flows often occur in the ocean, the atmospheric boundary layer, and in many industrial operations, and the diffusions of scalars such as heat and mass in stratified flows are strongly affected by buoyancy. It is, therefore, of great practical interest to investigate the buoyancy effects on heat and mass transfer when predicting the turbulent diffusion of scalar quantities in the environment and designing industrial heat and mass transfer equipment. Extensive studies on buoyancy effects in density-stratified turbulent flows have been done in the past two decades, but complicated problems such as the eddy scales causing counter-gradient scalar transfer in strongly stable stratification still need elucidation (Kaltenbach, Gerz & Schumann 1994).

Counter-gradient heat and momentum transfer in laboratories was first observed by Komori *et al.* (1983) in a thermally stratified open-channel water flow with weak shear. Stillinger, Helland & Van Atta (1983), Itsweire, Helland & Van Atta (1986) and Rohr *et al.* (1988) have also observed counter-gradient mass transfer in linearly salt-stratified grid-generated turbulence. However, the previous studies on homogeneously stratified water flows have not clarified the details of the counter-gradient scalar and momentum transfer mechanism. Komori *et al.* (1983) studied only the time-averaged turbulence quantities such as heat and momentum fluxes and their correlation coefficients, but they did not investigate the details of the counter-gradient transfer mechanism in the frequency domain. Rohr *et al.* (1988) measured the cospectra of instantaneous momentum and mass fluxes, but the cospectra in stable stratification were too scattered to precisely determine which scale motions contribute to counter-gradient transfer. In particular, the contribution of small-scale motions to counter-gradient scalar and momentum transfer was not fully discussed (Rohr *et al.* 1988). For air, Lienhard & Van Atta (1990), Yoon & Warhaft (1990), Jayesh, Yoon & Warhaft (1991) and Kanzaki & Ichikawa (1995) observed counter-gradient heat flux in unsheared thermally stratified grid-generated turbulent flows with both initial linear and step temperature profiles. They have shown that in strong stratification the large-scale motions contribute to counter-gradient heat transfer but the small-scale motions do not generate counter-gradient heat flux. They also have suggested that the influence of the Prandtl number on counter-gradient heat transfer should be investigated through comparisons with measurements in thermally stratified water flows.

On the other hand, a number of numerical and theoretical studies on stratified turbulent flows have been developed. Deissler (1962) first applied the linearized two-point correlation equations to homogeneous stratified weak turbulence, and he theoretically predicted the presence of counter-gradient scalar transfer in strong stratification. Further calculations have shown that the contributions of large- and small-scale motions to counter-gradient transfer are quite different for high and low Prandtl number flows. Komori *et al.* (1983) and Komori (1980) also used the same linearized two-point correlation equations and showed that the qualitative variations of the measured turbulence quantities with the local gradient Richardson

number are well explained by the two-point correlation equations. Hunt, Stretch & Britter (1988) applied a rapid distortion theory (RDT) to homogeneous stratified flows and they have shown similar dependencies of turbulence quantities on the local gradient Richardson number to Deissler's (1962) calculations. Recently Hanazaki & Hunt (1996) were stimulated by numerical simulations (Kaltenbach *et al.* 1994) and the present experimental results to predict the effects of the Prandtl number and initial turbulence spectra by analytically solving the RDT equations. Comparing qualitatively their calculations with the present measurements, they suggested that the counter-gradient scalar transfer spectra can be explained by linear processes.

Recently, some direct numerical simulations (DNS) were made of sheared and unsheared homogeneous thermally stratified flows with linear temperature and velocity profiles (Gerz, Schumann & Elghobashi 1989; Gerz & Yamazaki 1993; Holt, Koseff & Ferziger 1992) and a large-eddy simulation (LES) was also applied to stratified flows by Kaltenbach *et al.* (1994). The simulations predicted counter-gradient scalar and momentum fluxes and suggested the effects of molecular diffusivities on the counter-gradient transfer. However, the application of DNS to stratified water flows with high Prandtl or Schmidt numbers is still controversial because of the spatial resolution of the DNS. More recently Gerz & Schumann (1996) proposed a conceptual model for a homogeneous stratified flow, based on both the results of the LES (Kaltenbach *et al.* 1994) and measurements by Rohr *et al.* (1988), and they tried to explain the contribution of turbulent motions with different scales to counter-gradient scalar and momentum transfer as well as the influence of the Prandtl number. Although their conceptual model is given for a homogeneous stratified flow, it is of interest to examine whether it is also applicable to a slightly inhomogeneous mixing-layer type of stratified flow. Besides DNS, a number of turbulence closure models have been developed for stratified flows (e.g. Yamada & Mellor 1975; Andre *et al.* 1978; Gibson & Launder 1978; Schumann 1987). In order to examine the second- or third-order closure models, it will also be of importance to clarify experimentally the effects of molecular diffusivity on counter-gradient transfer.

In addition to the problem of counter-gradient transfer, the difference in the diffusion of active heat and passive mass is another interesting problem in thermally stratified flows. Pearson, Puttock & Hunt (1983) and Hunt (1985) first predicted the difference in the eddy diffusivities of active heat and passive mass. However, this problem has not been experimentally investigated in stratified flows where both active heat and passive mass are simultaneously diffused, since it has been very difficult to measure simultaneously instantaneous temperature, concentration and velocity.

Thus, precise measurements of counter-gradient scalar and momentum fluxes in strongly stratified water flows with high Prandtl or Schmidt numbers are required both to clarify the counter-gradient transfer mechanism and to examine the DNS, closure models or other models. The purpose of this study is, therefore, both to experimentally investigate the counter-gradient scalar and momentum transfer mechanism in a mixing-layer type of density-stratified water flow and to clarify the effects of molecular diffusivities of active scalars and mean shear on counter-gradient transfer. This study also aims to investigate the difference in the diffusion of active heat and passive mass in thermal stratification. The measurements were conducted using specially developed combination of laser-fluorescence, laser-Doppler, and thermo-resistance techniques with spatial resolutions far smaller than the dissipation scales. Preliminary results in unsheared thermally stratified water flows are presented in Komori, Nagata & Murakami (1996).

2. Experiments

Figure 1 shows the measuring system and test apparatus. The test apparatus used was a water tunnel made of polymethylemethacrylate (PMMA), 1 m in length and 0.1×0.1 m in cross-section. A turbulence-generating grid was installed at the entrance to the test section, and it was of round-rod, square-mesh, single-biplane construction. The mesh size M and the diameter of the rod d were 0.02 and 0.003 m, respectively. Two kinds of stratified water flows were generated in the test section downstream of turbulence-generating grids.

The first was a thermally stratified water flow with a Prandtl number of $Pr \approx 6$. For this stratified flow, cold and hot water were separately pumped up from two big storage tanks to the head tanks, and then passed through the contraction, which was separated by a splitter plate into upper and lower sections. The high-temperature water in the upper stream was heated by a boiler and the temperature was regulated in the storage tank by an electric heater connected to a thermometer. Thus, stable thermal stratification with an initial step temperature profile was formed behind the grids, and the step profile was used to get stronger stratification on the centreline of the test section than a linear profile. To investigate the difference in the diffusion of passive scalar (mass) and active scalar (heat) in thermal stratification, sodium fluorescein dye ($C_{20}H_{10}Na_2O_5$) of $Sc \approx 600$ was homogeneously premixed only into the upper high-temperature stream ($\overline{C_1}$ = const. and $\overline{C_2} = 0$ in figure 1*a*). Three stratified conditions, namely weak, moderate and strong stratification, were used and the initial temperature difference between upper and lower streams, $\overline{T_1} - \overline{T_2}$, corresponded to 3 K, 7 K and 15 K, respectively. Stronger thermal stratification with the initial temperature difference larger than 15 K could not be achieved, because of the significant heat release from the high-temperature stream to the ambient.

The second flow was a salt-stratified water flow with the active scalar (salt) having a high Schmidt number of $Sc \approx 600$. To make the salt-stratified flow, salt water with a constant concentration of NaCl ($\overline{C_2}$ = const.) was used for the lower stream, and fresh water ($\overline{C_1} = 0$) for the upper stream. The initial density differences between the upper and lower streams, $\Delta\overline{C}(= \overline{C_2} - \overline{C_1})$, were 18, 95 and 133 mol m^{-3} and they were prepared to correspond to the temperature differences of 3 K, 15 K and 20 K, respectively. To enable us to measure the instantaneous concentration of the active scalar (salt), sodium fluorescein dye was premixed with the fresh water in the upper stream. In this case, the salt concentration normalized by the initial concentration $\overline{C_2}$ was given by subtracting the sodium fluorescein dye concentration normalized by the initial concentration $\overline{C_1}$ from 1.0, since the Schmidt number is almost the same for the salt and the sodium fluorescein dye.

Mean velocities of the upper high-temperature and lower low-temperature streams, $\overline{U_1}$ and $\overline{U_2}$, were set to the same value of 12.5 cm s^{-1} for unsheared stratified flows, and for sheared stratified flows the initial velocity difference between upper and lower streams, $\Delta\overline{U}(= \overline{U_1} - \overline{U_2})$, was set to 2 or 3 cm s^{-1} by fixing the cross-sectionally averaged velocity $\overline{U}_{ave}$ to a constant value of 12.5 cm s^{-1}. Therefore, the Reynolds number based on the mesh size, Re_M, was 2500 for both unsheared and sheared flows. The turbulence Reynolds number based on the microscale, Re_t, was estimated to be about 20 at $x/M = 6$ for unsheared flows. To investigate the influence of the Reynolds number on the scalar transfer mechanism an unsheared thermally stratified water flow with $\overline{U}_{ave} = 25.0$ cm s^{-1} and $Re_t \approx 35$ was added. The experimental conditions including the Brunt–Väisälä frequency estimated at $x/M = 6$, N_0, are listed in table 1.

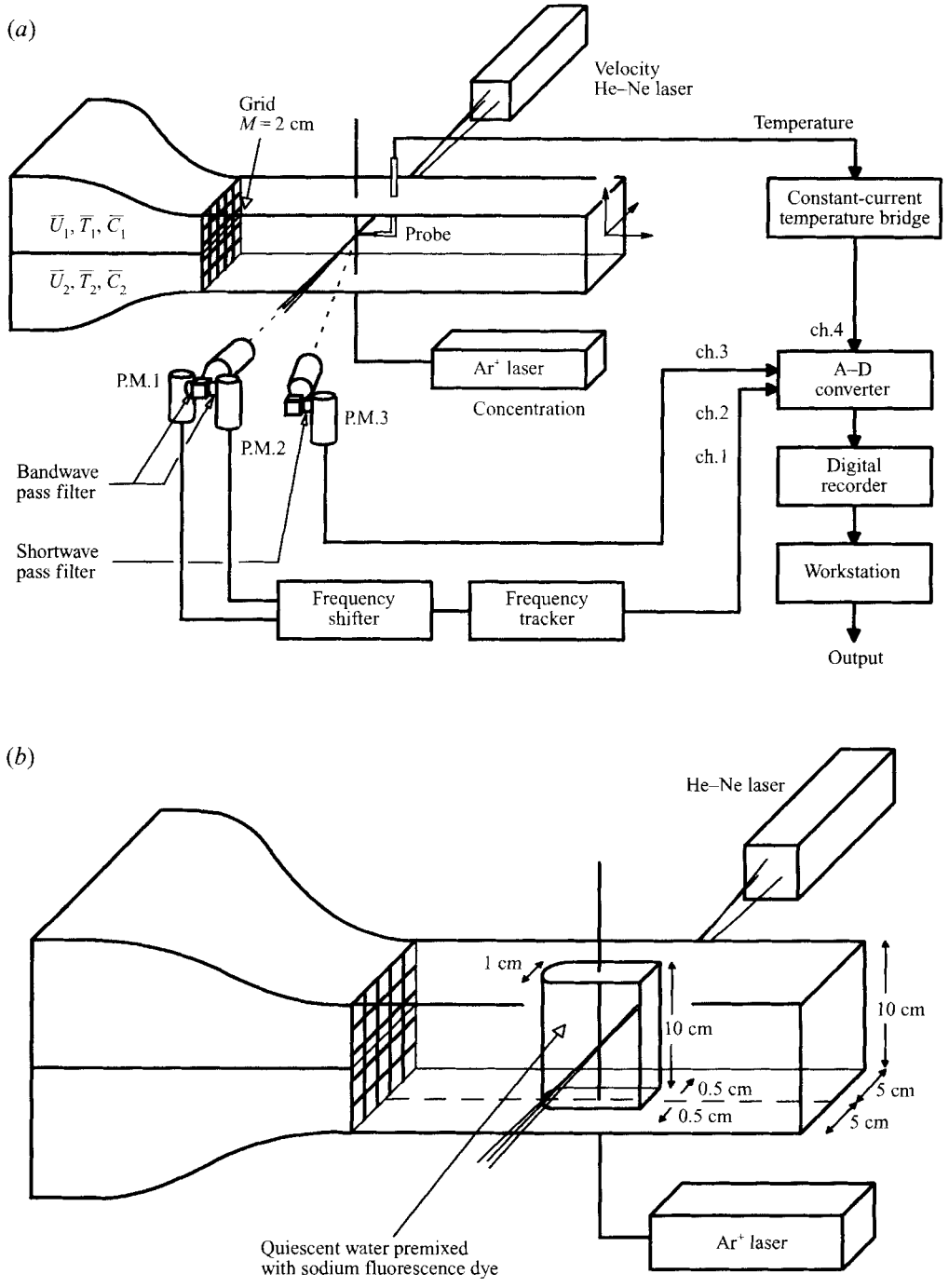

FIGURE 1. (*a*) Measuring system and test apparatus. (*b*) A small water cell for estimating the measurement errors due to the refractive index fluctuations in stratified flows.

Run No.	Active scalar	Passive scalar	$\overline{U}_{ave}$ (cm s^{-1})	$\Delta\overline{U}$ (cm s^{-1})	$\Delta\overline{T}$ (K)	$\Delta\overline{C}$ (mol m^{-3})	N_0 (s^{-1})	Re_M
1	heat ($Pr = 6$)	Sodium fluorescein	12.5	0.0	3.0	–	0.67	2500
2	heat ($Pr = 6$)	Sodium fluorescein	12.5	0.0	7.0	–	1.17	2500
3	heat ($Pr = 6$)	Sodium fluorescein	12.5	0.0	15.0	–	1.75	2500
4	heat ($Pr = 6$)	Sodium fluorescein	12.5	2.0	15.0	–	1.61	2500
5	heat ($Pr = 6$)	Sodium fluorescein	12.5	3.0	15.0	–	1.47	2500
6	heat ($Pr = 6$)	Sodium fluorescein	25.0	0.0	15.0	–	1.61	5000
7	salt ($Sc = 600$)	–	12.5	0.0	–	18.0	0.67	2500
8	salt ($Sc = 600$)	–	12.5	0.0	–	95.0	1.75	2500
9	salt ($Sc = 600$)	–	12.5	2.0	–	95.0	1.66	2500
10	salt ($Sc = 600$)	–	12.5	3.0	–	95.0	1.53	2500
11	salt ($Sc = 600$)	–	12.5	0.0	–	133.2	2.17	2500
12	salt ($Sc = 600$)	–	12.5	2.0	–	133.2	2.09	2500
13	salt ($Sc = 600$)	–	12.5	3.0	–	133.2	1.94	2500

TABLE 1. Experimental conditions.

Here, the Brunt–Väisälä frequency N is defined by $N = \left[-(g/\rho_0)(\partial\overline{\rho}/\partial y)\right]^{1/2}$, where ρ_0 is the bulk-averaged density.

Instantaneous velocities, temperature and concentration of passive mass in thermally stratified water flows were simultaneously measured using a combined measuring technique as shown in figure 1(*a*). For the salt-stratified flows, instantaneous velocities and salinity were simultaneously measured. The measuring technique combined a two-component laser-Doppler velocimeter with a resistance thermometer and a laser-induced fluorescence method. The laser-Doppler velocimeter used here was a DANTEC 55X Modular system with a polarization beam splitter (55X24), a 40 MHz Bragg cell and a beam expander, and the laser was a 5 mW He-Ne laser with a 632.8 nm wavelength (Spectra Physics Model 106-1). For temperature measurements, a cold-film I-probe of 10 μm diameter (TSI 1260-10W) operated by a constant-current temperature bridge (DANTEC 55M) was used, and it was located just behind the measuring point of velocity and concentration. A gap of about $\lambda = 0.5$ mm between velocity and temperature measuring points was compensated by giving a time lag of $\lambda/\overline{U}$ to the time records of the instantaneous temperature. For concentration measurements, a laser-induced fluorescence method was used, and the sodium fluorescein dye diffusing in the flow was illuminated by a high-power single-line mode argon-ion (Ar^+) laser of 0.8 W power and a 488 nm wavelength (LEXCEL model 95-4). The He-Ne laser beams for velocity measurements were shone from the sidewall of the test section, and a single-beam of an Ar^+ laser for concentration measurements was shone from the bottom wall. Both beams were focused by convex lenses and intersected perpendicularly at a measuring point. The fluorescence from the measuring point was collected using an optical system (DANTEC 55X34). The focused and magnified fluorescence passed through a pinhole of 0.1 mm diameter, and it was received by a photomultiplier (HAMAMATSU R-777). The Doppler signals for velocity measurements were collected by another optical system (DANTEC 55X34) connected to photomultipliers (DANTEC 55X08). The wavelength difference between the Doppler signals from the scattered particles and the fluorescence from the sodium fuorescein dye was about 100 nm and therefore the two lights could be separated by installing optical filters between the optical system and the photomultiplier. Short-wave and bandwave pass filters were installed in front of the photomultipliers for the

concentration and velocity measurements, respectively. The details of the spectra of fluorescence and scattered light, transmittance of optical filters and spatial resolution are described in Komori *et al.* (1993). The spatial resolutions of velocity, temperature and concentration measurements were 1.2 mm, 500 μm and 120 μm, respectively, and they were far smaller than the dissipation scales of velocity, temperature and concentration fluctuations estimated from their dissipation spectra.

The measurements were made mainly on the centreline in the region $6 \leqslant x/M \leqslant 20$. The sampling interval and the sample size were 0.00025 s and 240 000, respectively, and this gave reliable statistics. Statistical processing of the digitized data was done by a computer (SUN SPARC 10).

In addition, flow visualization was done to investigate the flow structure. The laser-induced fluorescence method using sodium fluorescein dye and a vertical Ar^+-laser sheet was used.

For velocity and concentration measurements by a non-contacting laser technique in a density-stratified flow, measurement errors due to refractive index fluctuations should be carefully estimated. Fluctuating movements of a laser beam at a receiver point are generated by integrating the effects of the density fluctuations along two light paths between an incident point and a measurement point and between a measurement point and a receiver point. Therefore, the effects of the refractive index fluctuations on the present laser technique depend on both the turbulence structure and density gradients along the light paths in stratified flows. Thus, the best way for approximately estimating the errors is to measure apparent velocity and concentration fluctuations due to the refractive index fluctuations by using a small isolated water cell fixed in a density-stratified flow (see figure 1*b*), and then to compare the apparent fluctuations with the velocity and concentration fluctuations measured in a normal stratified flow without using the water cell.

A small cell with the spanwise thickness of 1 cm, made of a thin polymethylemethacrylate plate, was vertically fixed along the centreline of the test section floor (figure 1*b*). To equate a distance between the sidewall of the small water cell and the wall of test section to a distance between a normal measurement point and the sidewall of the test section, the water cell was located at $z = +0.5$ cm or $z = -0.5$ cm from the centreline of the test section. The estimation of the errors was conducted for these two locations. Water premixed homogeneously with sodium fluorescence dye was quiescently put in the cell, and this quiescent water did not have velocity and concentration fluctuations. However, when the quiescent water cell is put in a stratified flow, the refractive index fluctuations along receiving and incident light paths in the ambient stratified flow generate apparent velocity and concentration fluctuations despite the quiescent water in the cell. The comparisons between the apparent and normal measurements have shown that the measurement errors due to the refractive index fluctuations are 0.3% and 0.7% for the mean squared values of velocity and concentration fluctuations, respectively. Thus, the accuracy of the present combined laser-Doppler and laser-induced fluorescence technique was satisfactory for this study.

However if this kind of non-contacting laser measurement technique is applied to a more three-dimensional density-stratified turbulence such as density-stratified oscillating-grid-induced turbulence (e.g. Fernando 1988) than the present mixing-layer type of stably stratified flow, greater errors may be generated even for small density gradients, since a great number of grid-generated energy-containing eddies along light paths cause significant refractive index fluctuations. In this case, we will need a sophisticated matching method for the refractive index such as used in

Hannoun, Fernando & List (1988). However, for a thermally stratified mixing flow, it is inherently impossible to apply such a matching method based on the usage of alcohol as in Hannoun *et al.* (1988), since the difference in molecular diffusivities of heat and alcohol is quite large. To demonstrate these points, we estimated the measurement errors in an unstably stratified flow with an initial temperature difference of 15 K by using the above small isolated water cell. An unstably stratified flow was produced in the present apparatus by replacing the high-temperature upper stream by the low-temperature lower stream, and the mean temperature gradient in the vertical direction was smaller than that in the present stably stratified flow but with the same initial temperature difference of 15 K. The measurement errors were 10% for the mean-squared values of both velocity and concentration fluctuations and they were much greater than those in the present stably stratified flow with the same initial temperature difference. This fact showed that despite the same initial temperature difference and small temperature gradients the errors due to the refractive index fluctuations are quite different for stably and unstably stratified flows, depending on the turbulence structure. Thus, it should be noted that whether a non-contacting laser technique is applicable to a density-stratified flow cannot be determined only from the magnitude of the mean density gradient: measurement errors should also be estimated by the present method based on the usage of a small isolated water cell.

Besides the errors due to refractive index fluctuations along light paths, signal dropout due to the movements of the measuring volume may occur in a large-density-gradient flow. Of course, the erroneous signals due to small movements of the measuring volume that do not cause signal dropout could be approximately estimated by using the above small isolated water cell. However, when the movements of the measuring volume are violent, they prevent us from catching the measuring volume in the pinhole of a photomultiplier and they result in signal dropout. For such violent movements, the present non-contacting laser technique cannot be applied with a satisfactory accuracy. Fortunately, for the present stratified flows with low turbulence and initial temperature differences of less than 20 K, the change of the signal dropout ratio was negligibly small compared to neutrally stratified flows. Thus, we could avoid the problem of signal dropout in the present stratified flows.

3. Results and discussion

3.1. *Counter-gradient scalar transfer in unsheared stratified flows*

Figure 2 shows typical vertical profiles of the mean temperature and salinity at the locations $x/M = 6$, 14 and 20 in unsheared strongly stratified flows ($N_0 = 1.75$ s^{-1}). Here N_0 is the value of the Brunt–Väisälä frequency N at $x/M = 6$. In the central region $|y/M| < 0.2$, both temperature and salinity profiles are rather close to linear profiles.

Figure 3 shows the streamwise distributions of the vertical fluxes of the active heat and salt in unsheared thermally and salt-stratified flows, normalized by the product of the mean velocity $\overline{U}$ and the initial temperature or concentration difference, $\Delta\overline{T}(= \overline{T_1} - \overline{T_2})$ or $\Delta\overline{C}(= \overline{C_2} - \overline{C_1})$. They are shown for four stratified conditions with $N_0 = 0.67$, 1.17, 1.75 and 2.17 s^{-1}. Both the heat and salt fluxes are suppressed with increasing stability. In strong stratification ($N_0 \geqslant 1.75$ s^{-1}), both the heat and salt fluxes change their signs despite the persistent negative mean-density gradients in the upward direction (see figure 2). This means that counter-gradient heat and salt transfer occurs in the strong stratification. In particular the counter-gradient salt flux

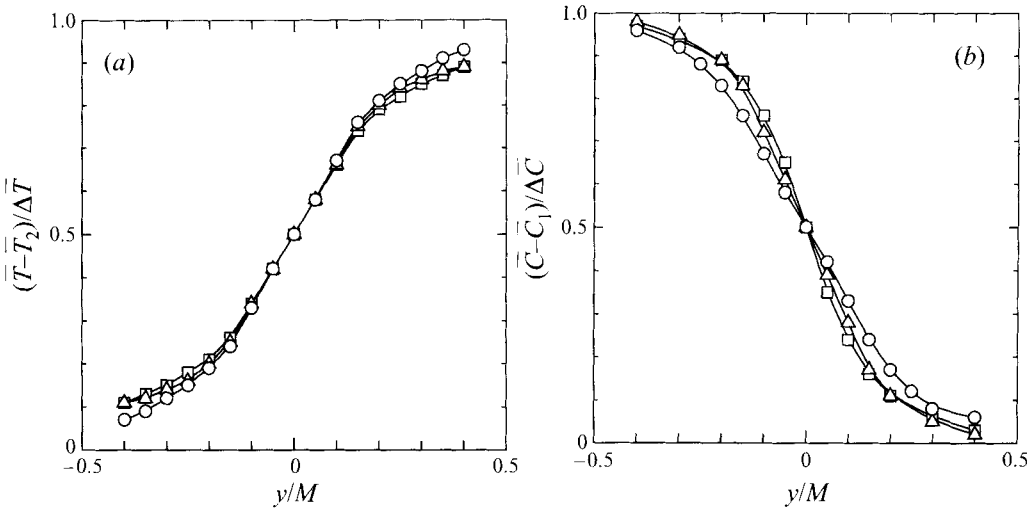

FIGURE 2. Typical vertical profiles of the mean (*a*) temperature and (*b*) salinity in unsheared strongly stratified water flows (N_0 = 1.75 s^{-1}): ○, x/M=6; △ , x/M=14; □, x/M=20.

is more notable than the heat flux even for the same Brunt–Väisälä frequency of N_0 = 1.75 s^{-1}. This difference will be discussed later together with the effects of molecular diffusion on counter-gradient transfer. When we replot the heat and salt fluxes in correlation coefficient form against the local dimensionless time $Nt(= Nx/\overline{U})$, the distributions of $R_{v\theta}(= \overline{v\theta}/v'\theta')$ and $R_{vc}(= \overline{vc}/v'c')$ can be shown for $Nt < 4$ by an unique curve, as shown in figure 4.

To investigate the counter-gradient scalar transfer mechanism, the joint probability density function (p.d.f.) of the vertical velocity fluctuation v and temperature fluctuation θ was computed and the distributions of the p.d.f.s at x/M = 14 are shown in figure 5 for unsheared weakly and strongly stratified flows. In weak stratification where the down-gradient transfer ($-\overline{v\theta} > 0$) is dominant, the p.d.f. prevails in the second and fourth quadrants (figure 5*a*), whereas in strong stratification the p.d.f. strengthens almost equally in the first and third quadrants (figure 5*b*). This means that counter-gradient heat transfer is generated by both the upward motion of the hot fluid and the downward motion of the cold fluid (Gerz *et al.* 1989). The behaviour of the p.d.f. of v and θ was quite similar to that of v and c in salt-stratified water flows.

In addition to the joint probability density functions, figures 6 and 7 show the normalized conditional heat and salt fluxes in weakly and strongly stratified flows. The conditional fluxes $\langle v\theta|\theta\rangle$ and $\langle vc|c\rangle$ are defined by the conditionally averaged fluxes for a temperature fluctuation θ and a concentration fluctuation c (see Jayesh & Warhaft 1994). For weakly stratified flows, the conditional fluxes follow inverted parabolas well:

$$\langle v\theta|\theta\rangle/|\overline{v\theta}| = -(\theta/\theta')^2, \tag{3.1}$$

and

$$\langle vc|c\rangle/|\overline{vc}| = -(c/c')^2. \tag{3.2}$$

The inverted parabolas can be derived from joint normal distributions of v and θ and v and c for a passive linear scalar profile in isotropic grid turbulence (see Jayesh & Warhaft 1994). In strong stratification, the conditional fluxes deviate

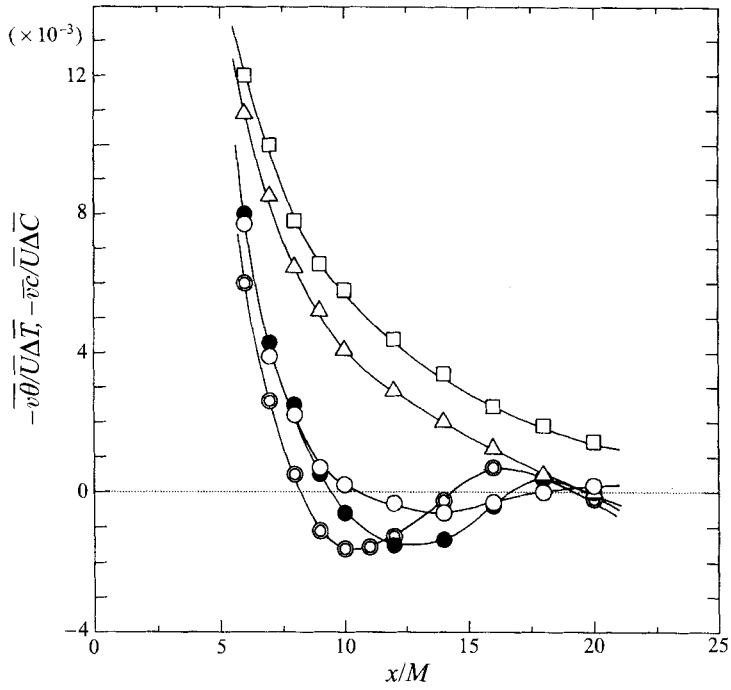

FIGURE 3. Streamwise distributions of the normalized vertical fluxes of the active heat and salt in unsheared thermally and salt-stratified water flows: □, heat flux for $N_0 = 0.67$ s^{-1}; △, heat flux for $N_0 = 1.17$ s^{-1}; ○, heat flux for $N_0 = 1.75$ s^{-1}; ●, salt flux for $N_0 = 1.75$ s^{-1}; ◎, salt flux for $N_0 = 2.17$ s^{-1}.

considerably from inverted parabolas, and $\langle v\theta|\theta\rangle$ and $\langle vc|c\rangle$ become positive in the region $|\theta/\theta'| > 0.5$ and $|c/c'| > 0.5$, whereas the conditional heat flux of Jayesh & Warhaft (1994) in thermally stratified air flows becomes positive only in the region $|\theta/\theta'| > 3$. The difference suggests that the counter-gradient scalar transfer in stratified water flows is far larger than in stratified air flows.

Thus, it is found that counter-gradient scalar transfer in strong stratification is generated by both the upward motion of the low-density fluid and the downward motion of the high-density fluid. The buoyancy-induced motions obviously promote the intensity of the vertical velocity fluctuations in the region $x/M > 10$ as shown in figure 8, whereas the intensity of the longitudinal velocity fluctuation hardly changes compared to the neutral case.

To find at what scale the counter-gradient scalar transfer occurs, the cospectra of v and θ, $Cs_{v\theta}$, were computed. Figure 9 shows the cospectra of v and θ at the four locations $x/M = 6$, 10, 14 and 16 under the three stratified conditions $N_0 = 0.67$, 1.17 and 1.75 s^{-1}. The cospectra at $x/M = 10$ and 14 in strong thermal stratification ($N_0 = 1.75$ s^{-1}) are magnified in figure 9(*d*) for clear comparison. The area of the cospectra multiplied by the frequency f indicates the quantity of heat flux, and negative and positive values of $Cs_{v\theta}$ correspond to down-gradient heat flux and counter-gradient heat flux, respectively. In weak stratification ($N_0 = 0.67$ s^{-1}) the cospectra at all locations are always negative in the whole frequency region (figure 9*a*). The negative cospectra show that at all scales down-gradient transfer is dominant in weak stratification. In strong stratification ($N_0 = 1.75$ s^{-1}), the cospectrum starts to change its sign from the higher frequency range at $x/M = 10$ and the cospectrum

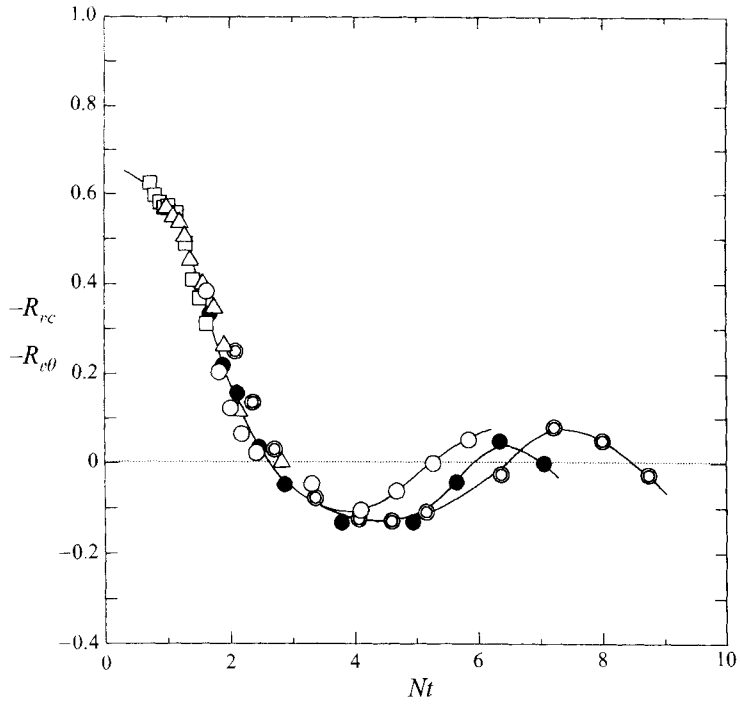

FIGURE 4. Time variations of the correlation coefficients of the vertical fluxes of the active heat and salt in unsheared thermally and salt-stratified water flows. Symbols as in figure 3.

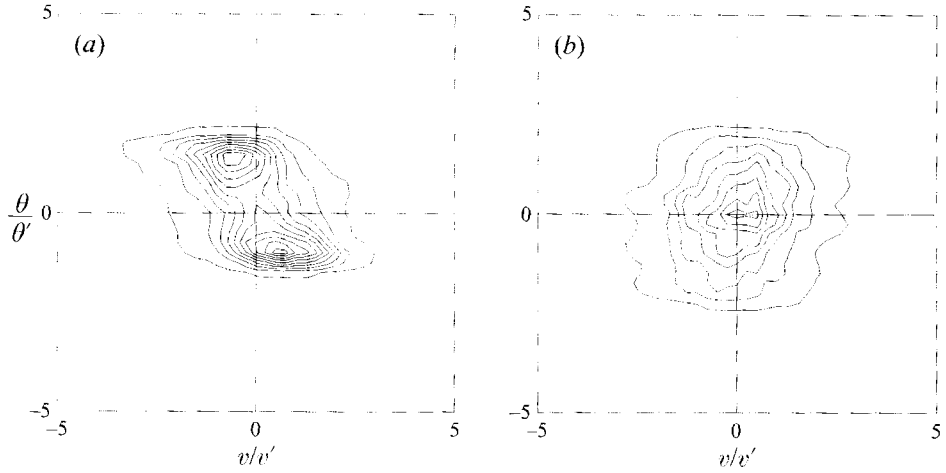

FIGURE 5. Joint probability density function of the vertical velocity and temperature fluctuations at x/M=14: (*a*) in weak thermal stratification (N_0 = 0.67 s^{-1}); (*b*) in strong thermal stratification (N_0 = 1.75 s^{-1}).

at x/M = 14 becomes positive in the whole frequency range (figure 9*c*,*d*). This means that in strong stratification counter-gradient transfer first becomes dominant at small scales and then it spreads to large scales. In fact the flow visualization based on the laser-induced fluorescence technique shows that the small-scale motions (buoyancy-induced upward and downward finger-like structures), returning to their

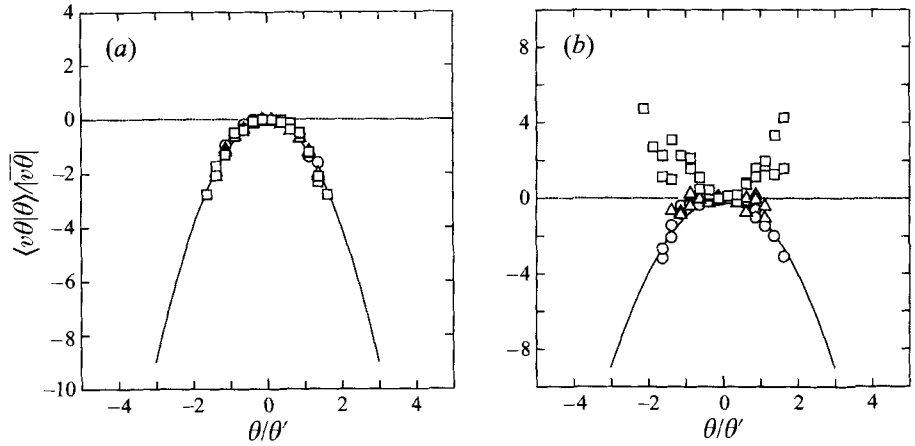

FIGURE 6. The normalized conditional heat flux in unsheared (*a*) weakly ($N_0 = 0.67$ s^{-1}) and (*b*) strongly ($N_0 = 1.75$ s^{-1}) thermally stratified flows: ○, x/M=6; △, x/M=10; □, x/M=14. The solid line shows equation (3.1).

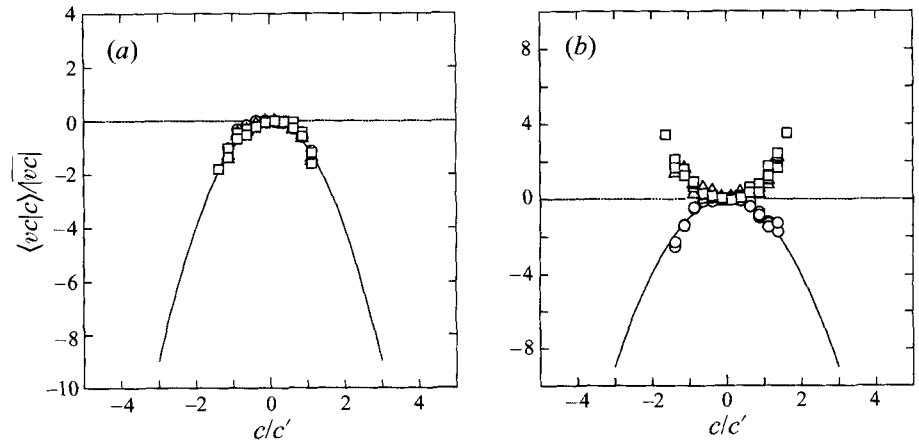

FIGURE 7. As figure 6 but for the normalized conditional salt flux in unsheared salt-stratified flows. The solid line shows equation (3.2).

original levels, are generated in the region near $x/M = 10$ (see the elongated tail indicated by an arrow in figure 10) and the large-scale motions are pushed back by buoyancy to their original levels in the region near $x/M = 14$. At $x/M = 16$ in strong stratification, the counter-gradient heat flux begins to decrease (figure 9*c*) and this results in an oscillation of the heat flux in figure 3. The time oscillation of the counter-gradient scalar flux appears more clearly in the cospectra of v and c in very strong salt-stratification as shown in figure 11. The counter-gradient flux oscillates at large scales, but the counter-gradient flux at small scales persists without oscillating. This qualitatively agrees with Gerz & Schumann (1991).

When we deduce the buoyancy-driven motions from the above results (figures 3, 5 and 9), we obtain a sketch of the buoyancy-driven motions in strong stratification, as shown in figure 12. In the initial mixing region $x/M \approx 6$, the vertical turbulence kinetic energy (VKE $= \overline{v^2}/2$) in strong stratification ($N_0 = 1.75$ s^{-1}) is comparable

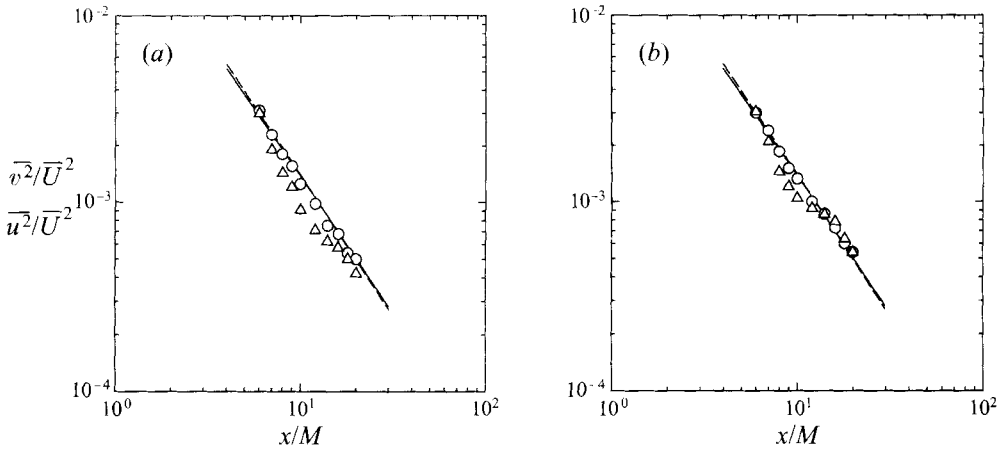

FIGURE 8. Streamwise distributions of the turbulence intensities of the vertical and longitudinal velocity fluctuations in unsheared strongly (*a*) thermally and (*b*) salt-stratified flows ($N_0 = 1.75\ \mathrm{s}^{-1}$): ○, $\overline{u^2}/\overline{U}^2$; △, $\overline{v^2}/\overline{U}^2$. The solid and dashed lines show $\overline{u^2}/\overline{U}^2$ and $\overline{v^2}/\overline{U}^2$ in the neutrally stratified flow, respectively.

to the available potential energy (APE $= \beta g\overline{\theta}^2/\frac{1}{2}(\partial\overline{T}/\partial y)$; $\partial\overline{T}/\partial y =$ constant in the central region $|y/M| < 0.2$ (Holliday & McIntyre 1981)) as shown in figure 13, and therefore the turbulent motions which are responsible for the down-gradient transfer are still predominant (figure 12*a*). However, the turbulence decays, and at about $x/M \approx 10$, the available potential energy becomes larger than the turbulence energy. When we consider the mean field production and buoyancy production terms in the transport equation of the heat flux $-\overline{v\theta}$:

$$\frac{\mathrm{D}}{\mathrm{D}t}\left(-\overline{v\theta}\right) = \overline{v^2}\frac{\partial\overline{T}}{\partial y} - \beta g\overline{\theta^2} + (\alpha+\nu)\,\overline{\frac{\partial\theta}{\partial x_i}\frac{\partial v}{\partial x_i}} + \overline{\frac{p}{\rho}\frac{\partial\theta}{\partial y}} - \frac{\partial}{\partial x_i}\left(\overline{vu_i} + \overline{\frac{p\theta}{\rho}}\delta_{2i}\right), \qquad (3.3)$$

we can infer that the relative increase of APE with respect to VKE causes the counter-gradient transfer. Of course, there exists a time delay between the relative increase of APE and the change of the sign of $-\overline{v\theta}$ (figure 3) because of buffer effects due to other terms on the right-hand side in (3.3). The ratio of the spectrum of APE to that of VKE, S_{APE}/S_{VKE}, is shown for two stratified cases in figure 14. The ratio of APE to VKE first increases at small scales upstream of the region of counter-gradient heat flux in figure 3, and then it rapidly increases at large scales. The reason why APE/VKE first increases at small scales lies in the fact that for high Prandtl numbers greater than 1.0 the dissipation rate of velocity fluctuation is faster than that of temperature fluctuation. The relative increase of APE at small scales induces small-scale upward and downward finger-like motions of the low- and high-density fluids, respectively, and the counter-gradient heat transfer due to the finger-like motions results in the positive cospectra in the high-frequency region in figure 9. The DNS by Nagata & Komori (1996) and Komori (1996) showed very similar results for APE/VKE and S_{APE}/S_{VKE} to these measurements. In addition to the small-scale motions, the large-scale motions are also strongly affected by buoyancy (see the rapid increase of APE in figure 14 and rapid decrease of the down-gradient heat flux at large scales in figure 9) (Gibson 1981). However, the large-scale energy-containing motions generating the down-gradient transfer are still dominant compared to the large-scale buoyancy-driven motions contributing to the counter-gradient transfer in

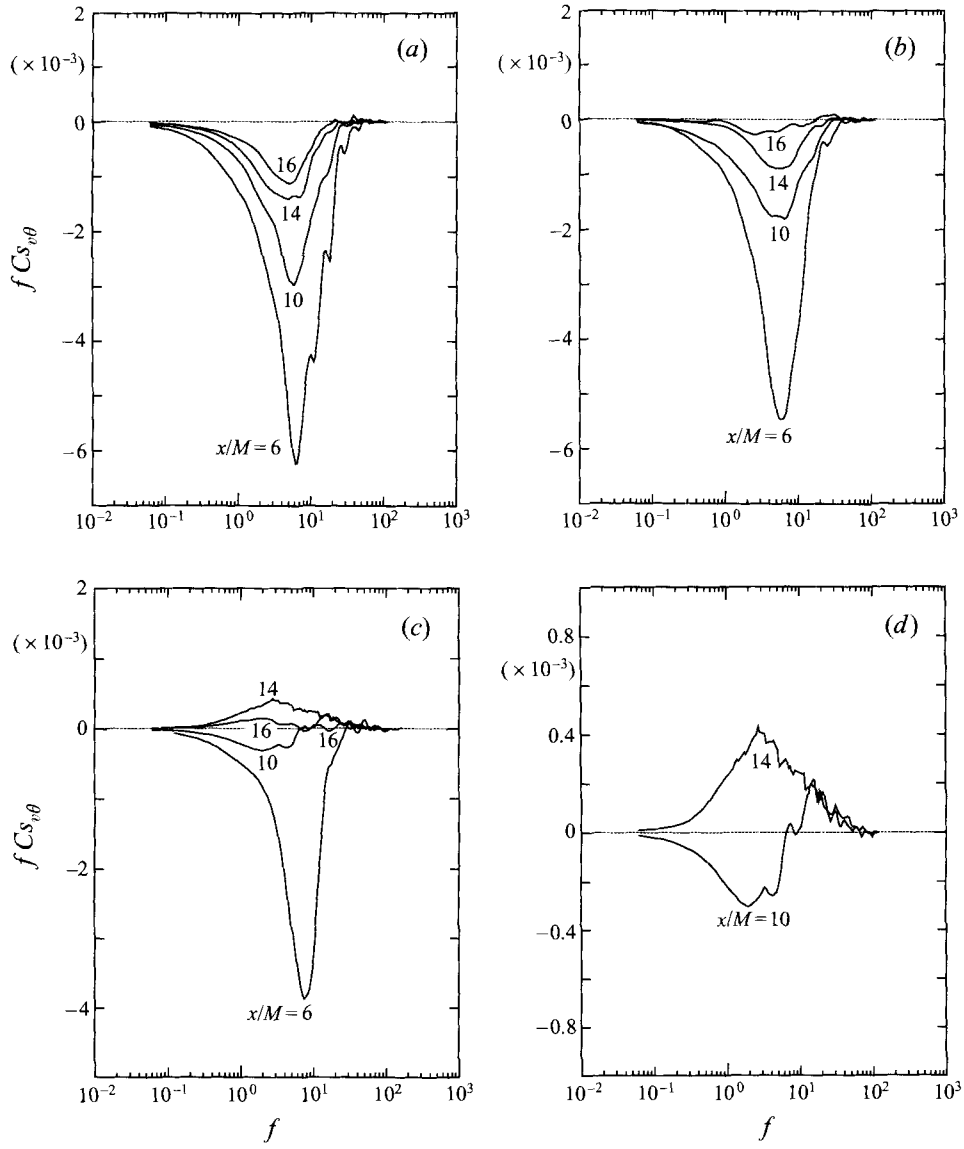

FIGURE 9. Cospectra of the vertical velocity fluctuation and temperature fluctuation: (*a*) in weak thermal stratification ($N_0 = 0.67$ s^{-1}); (*b*) in moderate thermal stratification ($N_0 = 1.17$ s^{-1}); (*c*) in strong thermal stratification ($N_0 = 1.75$ s^{-1}); (*d*) magnified distributions in strong thermal stratification ($N_0 = 1.75$ s^{-1}). The cospectra are normalized by $\overline{U}\Delta\overline{T}$.

the region $x/M < 10$ (figure 12*b*) and therefore the change in the sign of the heat flux at large scales occurs later than at small scales (figure 12*c*). In the region downstream of $x/M > 10$, buoyancy-driven motions are dominant at both small and large scales. This generates the positive values of the cospectra in the whole frequency region in figures 9(*c*) and 9(*d*).

The counter-gradient scalar transfer mechanism is the same for the thermally stratified water flow with the high Prandtl number and the salt-stratified flow with the high Schmidt number. However, the contributions of the small-scale and large-scale

FIGURE 10. Photograph of the fluid motions visualized by the laser-induced fluorescence method in the region $10 < x/M < 14$. An arrow indicates the small-scale finger-like structure.

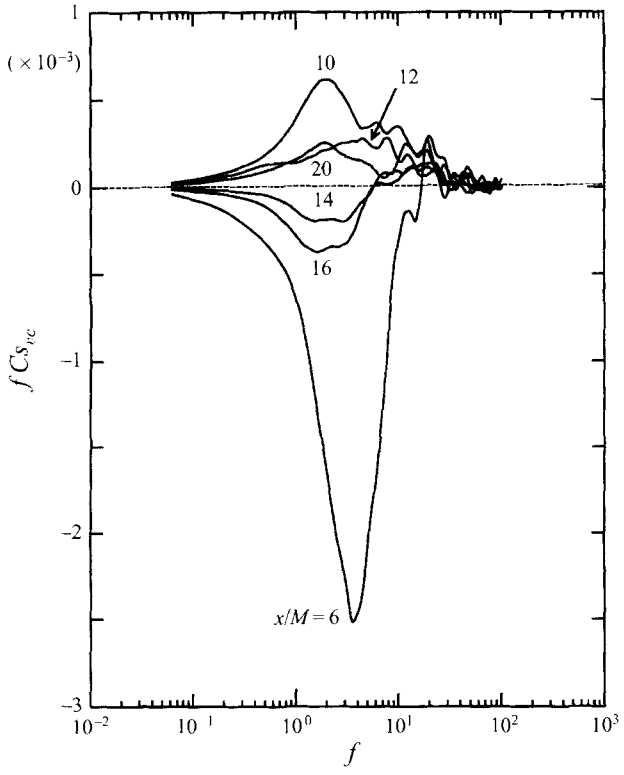

FIGURE 11. Cospectra of the vertical velocity fluctuation and concentration fluctuation in very strong salt-stratification ($N_0 = 2.17\ \mathrm{s}^{-1}$). The cospectra are normalized by $\overline{U}\Delta\overline{C}$.

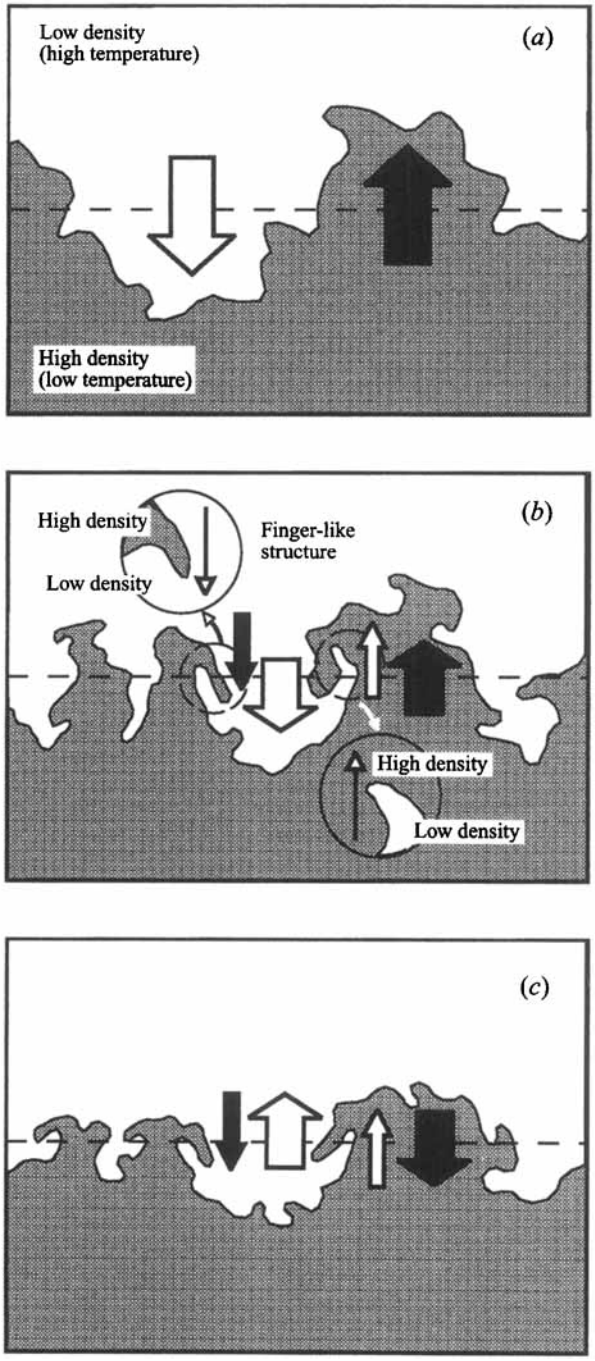

FIGURE 12. Sketch of the buoyancy-driven motions that contribute to the counter-gradient scalar transfer in strong stratification ($N_0 = 1.75\ \mathrm{s}^{-1}$): (*a*) at $x/M = 6$; (*b*) at $x/M = 10$; (*c*) at $x/M = 14$.

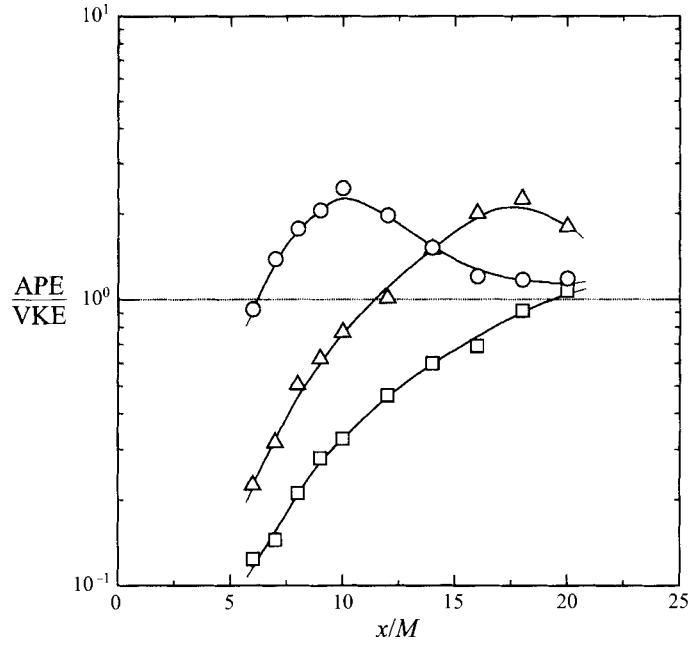

FIGURE 13. The ratio of the available potential energy to the vertical turbulence kinetic energy in thermal stratification: □, $N_0 = 0.67\ s^{-1}$; △, $N_0 = 1.17\ s^{-1}$; ○, $N_0 = 1.75\ s^{-1}$.

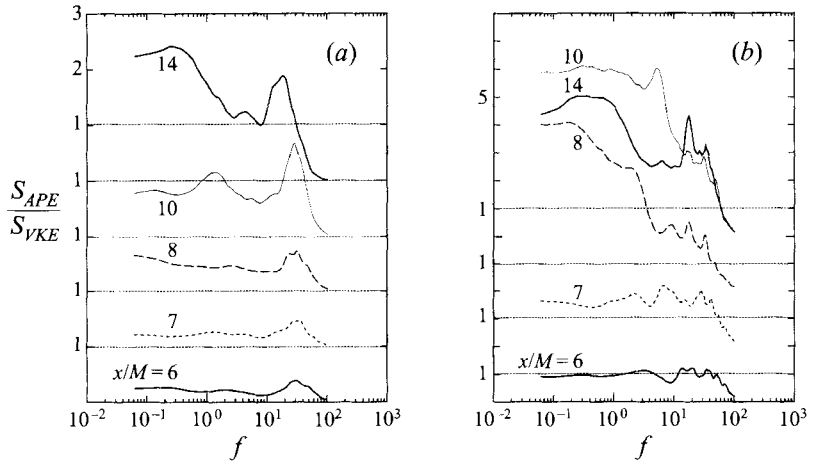

FIGURE 14. The ratio of the spectrum of the available potential energy to that of the vertical turbulence kinetic energy: (*a*) $N_0 = 1.17\ s^{-1}$; (*b*) $N_0 = 1.75\ s^{-1}$.

motions to the counter-gradient scalar fluxes are quite different for the unsheared stratified water flows in this study and the unsheared thermally stratified air flows in the previous studies, as shown for the profiles of the cospectra of v and θ in figure 15. In the unsheared homogeneous stratified air flows with low Prandtl numbers of $Pr \approx 0.7$ (Lienhard & Van Atta 1990; Yoon & Warhaft 1990; Jayesh *et al.* 1991), the counter-gradient heat flux due to the small-scale finger-like motions was not seen (figure 15*d–f*), since the relative molecular diffusion of heat is faster for air than for water (see the sketch in figure 16). That is, small-scale buoyancy-driven motions cannot

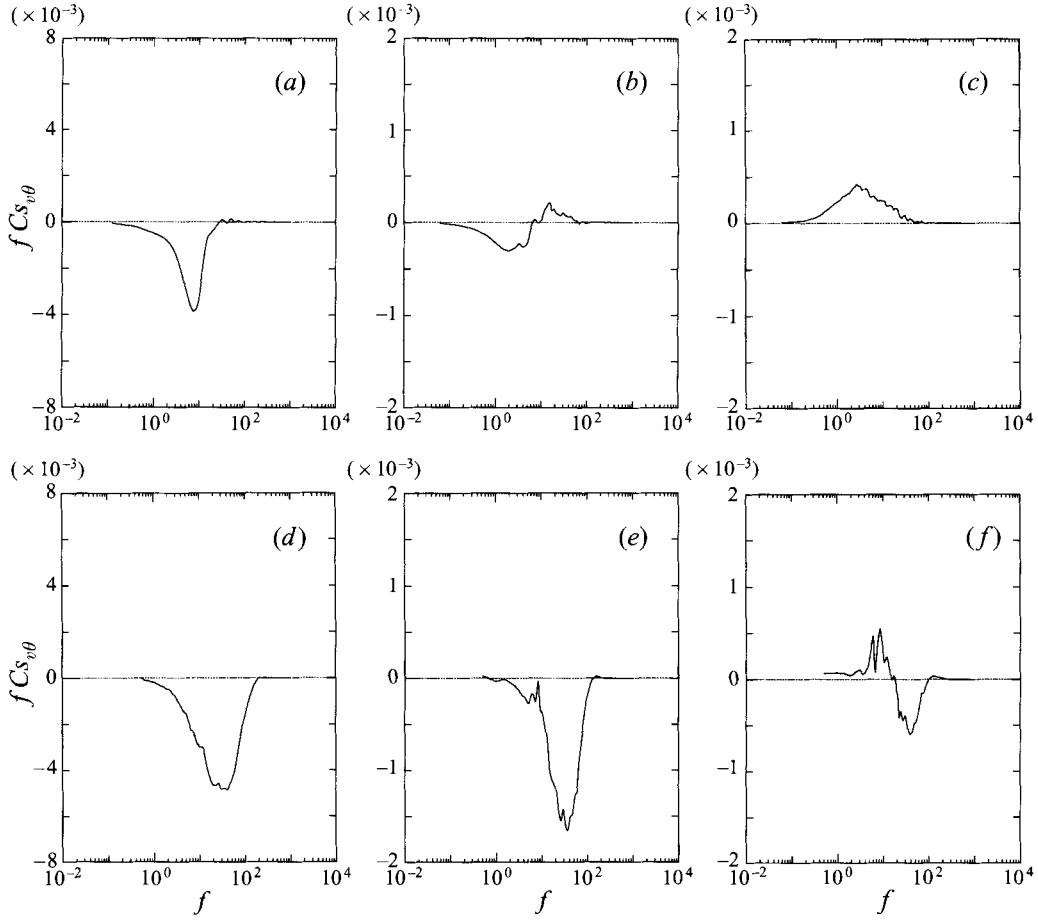

FIGURE 15. Comparison of the cospectra of v and θ between unsheared thermally stratified water and air flows versus the dimensionless time Nt: (*a*) $Nt = 1.75$ in the stratified water flow with $N_0 = 1.75\ \mathrm{s}^{-1}$; (*b*) $Nt = 2.47$ in the stratified water flow with $N_0 = 1.75\ \mathrm{s}^{-1}$; (*c*) $Nt = 3.79$ in the stratified water flow with $N_0 = 1.75\ \mathrm{s}^{-1}$; (*d*) $Nt = 1.71$ in the stratified air flow (Lienhard & Van Atta 1990) (*e*) $Nt = 2.56$ in the stratified air flow (Lienhard & Van Atta 1990) (*f*) $Nt = 3.17$ in the stratified air flow (Lienhard & Van Atta 1990) The cospectra in (*a*)–(*c*) are normalized by $\overline{U}\Delta\overline{T}$.

be generated in air flows because of the large smearing effect of molecular diffusion. For air, counter-gradient heat transfer occurs only at large scales (figure 15*f*) and the small-scale motions always contribute to the down-gradient transfer even in the strong stratification with the counter-gradient total flux of $-\overline{v\theta} < 0$ (Lienhard & Van Atta 1990; Yoon & Warhaft 1990; Jayesh *et al.* 1991; Jayesh & Warhaft 1994). The difference in the counter-gradient scalar transfer mechanism due to the Prandtl number has been suggested by the numerical predictions for homogeneous stratified flows by Deissler (1962), Hunt *et al.* (1988) and Gerz *et al.* (1989). A RDT of Hanazaki & Hunt (1996) based on linear processes showed that in high Prandtl number ($Pr > 1$) flows the counter-gradient scalar flux is strengthened at high wavenumbers, while in low Prandtl number ($Pr < 1$) flows the counter-gradient flux at high wavenumbers is suppressed. Their results also showed that stronger counter-gradient transfer is generated for higher Prandtl numbers. Although our measurements showed significant

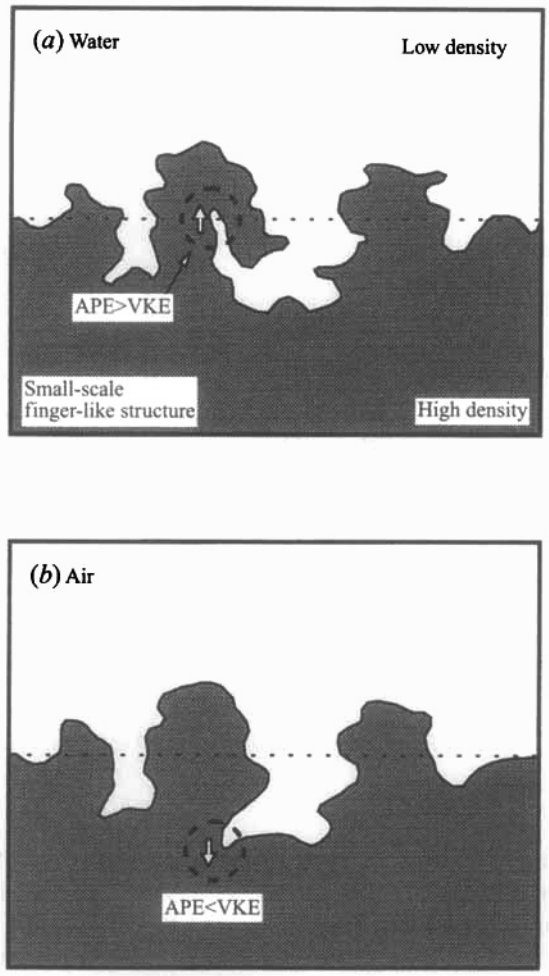

FIGURE 16. The difference in the small-scale motions of stratified water and air flows. (*a*) The buoyancy-induced finger-like motion contributes to the counter-gradient scalar transfer in the stratified water flow. (*b*) The small-scale finger-like motion is not generated because of the smearing effect of the molecular diffusion.

effects of the Prandtl or Schmidt numbers on counter-gradient transfer at all scales, they are in qualitative agreement with the calculations of Hanazaki & Hunt (1996).

In order to illuminate the influence of molecular diffusion on counter-gradient scalar transfer, the vertical turbulent fluxes of the active scalars are compared in three stratified flows with different molecular diffusivities in figure 17. Here the heat and salt fluxes are made dimensionless in the correlation coefficient forms of $R_{v\theta} = \overline{v\theta}/v'\theta'$ and $R_{vc} = \overline{vc}/v'c'$, and they are plotted against the dimensionless time Nt ($= Nx/\overline{U}$). The correlation coefficients intersect zero around $Nt = 2.5$. The value of $Nt = 2.5$ falls between $Nt \approx 2.0$ predicted and measured by Riley, Metcalfe & Weissman (1981), Hunt *et al.* (1988), Hanazaki & Hunt (1996) and Yoon & Warhaft (1990) and $Nt \approx 3.0$ measured by Lienhard & Van Atta (1990) and Itsweire *et al.* (1986) for homogeneous stratified flows. The counter-gradient scalar transfer is more pronounced for high Prandtl and Schmidt numbers and the salt flux with the highest Schmidt number verifies the oscillating behaviour $Nt > 3$ that has been predicted by the numerical simula-

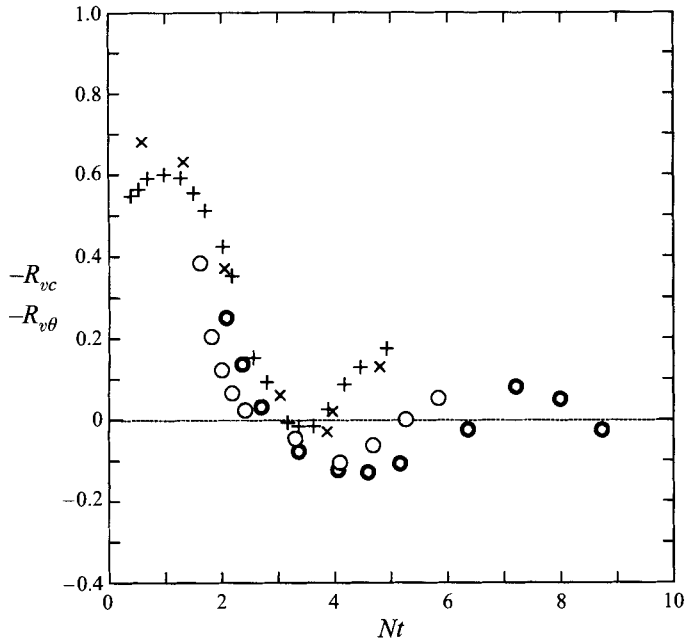

FIGURE 17. Comparisons of the correlation coefficients of the scalar fluxes between three unsheared stratified flows: ○, $R_{v\theta}$ in the thermally stratified water flow with $N_0 = 1.75$ s^{-1}; ◎, R_{vc} in the salt-stratified flow with $N_0 = 2.17$ s^{-1}; +, $R_{v\theta}$ in the thermally stratified air flow with $N_0 = 2.42$ s^{-1} (Lienhard & Van Atta 1990); ×, $R_{v\theta}$ in the thermally stratified air flow with $N_0 = 2.68$ s^{-1} (Jayesh *et al.* 1991).

tions. At the initial stage $Nt = 2 \sim 3$, the coefficients of the present heat and salt fluxes are close to the measurements of Lienhard & Van Atta (1990) and Jayesh *et al.* (1991) for air. In particular, it should be noted that the larger Prandtl number or Schmidt number lengthens the first buoyancy oscillating period of the counter-gradient fluxes. Thus, we can see the strong influence of molecular diffusion on counter-gradient transfer for $Nt > 3$, but it has been controversial whether it is the molecular diffusivity or the Reynolds number that has more influence on counter-gradient transfer (Gerz *et al.* 1989; Holt *et al.* 1992). It is especially uncertain whether counter-gradient scalar transfer at small scales is a characteristic of low Reynolds number flows that occur even in stratified air flow with $Pr \approx 0.7$. To investigate the influence of the Reynolds number, the cospectra of v and θ were measured in thermally stratified water flow with the higher Reynolds number of $Re_t \approx 35$ at $x/M = 6$ ($Re_M = 5000$) and the initial temperature difference of $\Delta\overline{T} = 15$ K (see table 1). The value of $Re_t \approx 35$ is close to that for most of the data obtained in the thermally stratified air flows of Lienhard & Van Atta (1990) and Jayesh *et al.* (1991). In the thermally stratified water flow with $Re_t \approx 35$, counter-gradient heat flux is not observed for $x/M < 20$ ($Nt < 2$) where the present measurements were limited, as shown in figure 18. However, it seems evident from the cospectrum at $x/M = 20$ in figure 19 that counter-gradient transfer begins to occur at small scales even for $Re_t \approx 35$. This together with the cospectra in Lienhard & Van Atta (1990) and Jayesh *et al.* (1991) suggests that counter-gradient scalar transfer at small scales is a mechanism characteristic of high Prandtl or high Schmidt number flow. Further our recent direct numerical simulations of thermally stratified air and water flows with the same turbulence Reynolds number (Nagata &

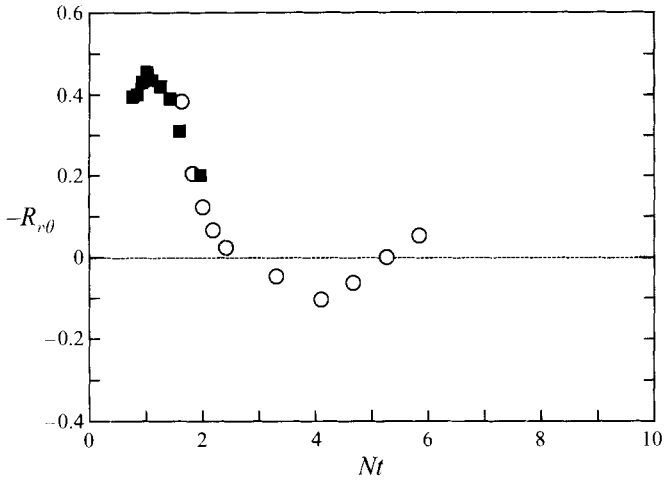

FIGURE 18. Correlation coefficient of the vertical heat flux in unsheared strongly thermally stratified flows with different Reynolds numbers: ○, $Re_t \approx 20$ and $Re_M = 2500$; ■, $Re_t \approx 35$ and $Re_M = 5000$.

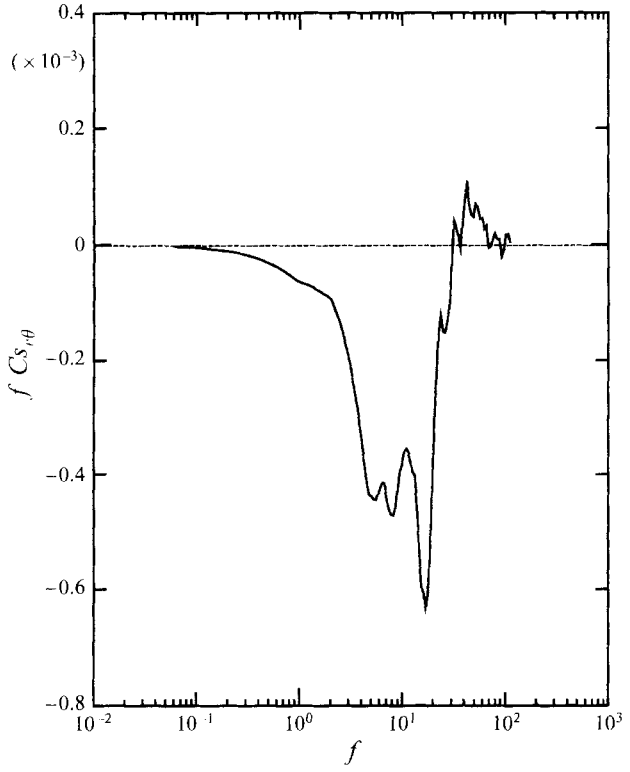

FIGURE 19. Cospectrum of the vertical velocity fluctuation and temperature fluctuation at $Nt = 2$ ($x/M = 20$ and $Re_t \approx 35$). The cospectrum is normalized by $\overline{U}\Delta\overline{T}$.

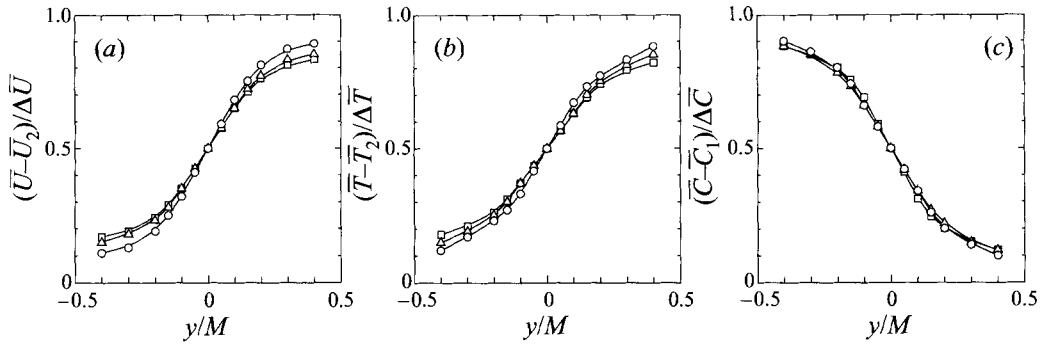

FIGURE 20. Typical vertical profiles of the mean (*a*) velocity, (*b*) temperature and (*c*) salinity in sheared thermally and salt-stratified flows with the initial velocity difference of $\Delta\overline{U} = 2$ cm s^{-1} and the initial density difference corresponding to $\Delta\overline{T} = 15$ K: ○, $x/M = 6$; △, $x/M = 10$; □, $x/M = 14$.

Komori 1996; Komori 1996) have predicted a quite similar influence of the Prandtl number on counter-gradient heat transfer. Also Gerz & Yamazaki (1993) predicted this influence of Pr. On the other hand, Gerz & Schumann (1991) suggested that for much higher turbulent Reynolds numbers counter-gradient transfer may occur at small scales even in a stratified air flow. When we consider the violent mixing at small scales in much higher turbulent Reynolds number flows, together with the generation mechanism of the counter-gradient scalar transfer (figure 12), we expect counter-gradient transfer in air at small scales. Although it may be difficult to get strong stratification in very high Reynolds number flows, it would be of interest to investigate counter-gradient transfer in a wind tunnel in a future study.

3.2. *Effects of mean shear on counter-gradient scalar and momentum transfer*

Figure 20 shows typical vertical profiles of the mean velocity together with mean temperature and salinity profiles in sheared thermally and salt-stratified flows with the initial velocity difference of $\Delta\overline{U} = 2$ cm s^{-1} and the initial density difference corresponding to $\Delta\overline{T} = 15$ K. Here $\Delta\overline{T} = 15$ K corresponded to a salinity difference of $\Delta\overline{C} = 95$ mol m^{-3}. For the present small velocity difference, the mean velocity, temperature and concentration profiles at $x/M \geqslant 6$ become almost linear in the central region $|y/M| < 0.2$, and therefore the present flow structure may be rather closer to that in a homogeneous stratified flow. In fact, flow visualization has shown that the structure of the roll-up characteristic of a mixing-layer flow appears clearly for $x/M < 4$ just behind turbulence-generating grids, but for $x/M \geqslant 6$ it rapidly disappears because of weak shear, as inferred from turbulence kinetic energy budget in figure 21. In the energy budget, each term is normalized by $\overline{U}^3/M$ and the dissipation was roughly estimated under the assumption of isotropic and frozen turbulence. The magnitude of the dissipation normalized by $\overline{u^2}\overline{U}/M$ was comparable to the previous measurements (Lienhard & Van Atta 1990; Itsweire *et al.* 1986; Stillinger *et al.* 1983). For reference the streamwise variations of the local gradient Richardson number are shown in figure 22. The variations are not large and therefore they show that the present stratified flows are close to sheared homogeneous stratified flows for $x/M > 9$.

Figures 23(*a*) and 23(*b*) show the streamwise distributions of the vertical heat and salt fluxes versus mean shear in thermally and salt-stratified water flows with the same initial density difference corresponding to $\Delta\overline{T} = 15$ K. Figures 24 and 25 show the cospectra of the vertical heat and salt fluxes at $x/M = 10$ and 14 in these sheared

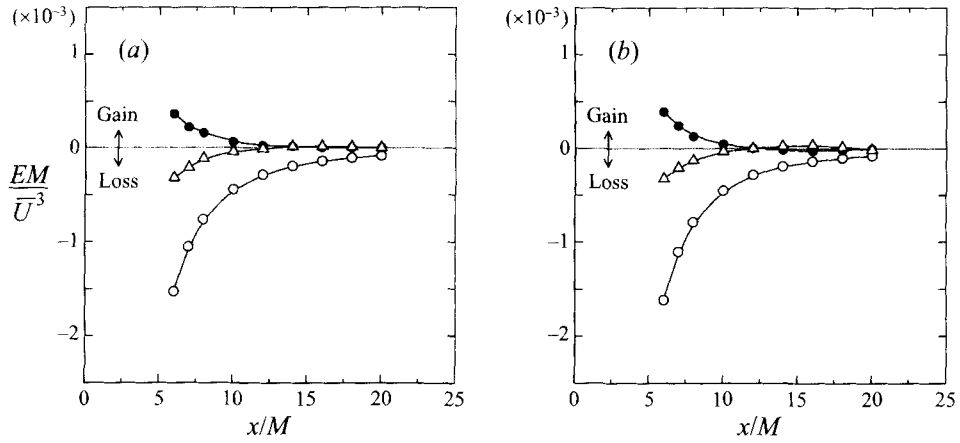

FIGURE 21. The normalized turbulence kinetic energy budget in sheared (*a*) thermally and (*b*) salt-stratified flows with the initial velocity difference of $\Delta\overline{U} = 2$ cm s^{-1} and the initial density difference corresponding to $\Delta\overline{T} = 15$ K: ○, viscous dissipation; ●, shear production; △, buoyancy production.

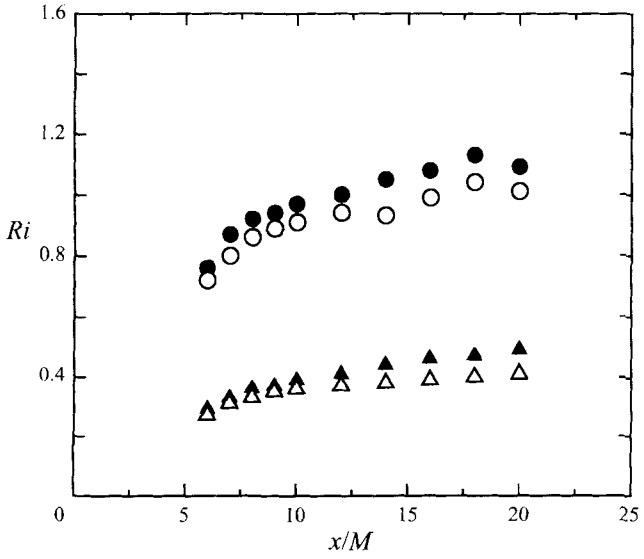

FIGURE 22. Streamwise distributions of the local gradient Richardson number in sheared thermally and salt-stratified flows with the initial velocity differences of $\Delta\overline{U} = 2$ cm s^{-1} and 3 cm s^{-1} and the initial density difference corresponding to $\Delta\overline{T} = 15$ K: ○, thermal stratification with $\Delta\overline{U} = 2$ cm s^{-1}; △, thermal stratification with $\Delta\overline{U} = 3$ cm s^{-1}; ●, salt stratification with $\Delta\overline{U} = 2$ cm s^{-1}; ▲, salt stratification with $\Delta\overline{U} = 3$ cm s^{-1}.

stratified flows. It is seen that the mean shear acts to reduce the counter-gradient scalar fluxes mainly at large scales. When the heat and salt fluxes are plotted against Nt as shown in figure 26, their fluxes are roughly correlated by a unique curve. Figures 27(*a*) and 27(*b*) show the normalized momentum fluxes with the scalar flux in sheared thermally and salt-stratified flows with the same initial density difference of $\Delta\overline{T} = 15$ K and $\Delta\overline{C} = 95$ mol m^{-3} and the initial velocity difference of $\Delta\overline{U} = 2$ cm s^{-1}. It should be emphasized that counter-gradient momentum transfer is more

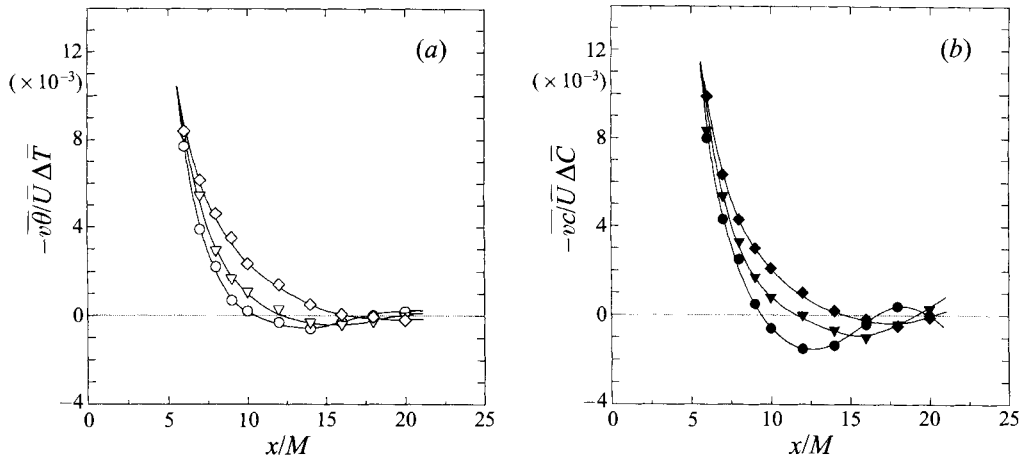

FIGURE 23. (*a*) Streamwise distributions of the normalized heat flux versus x/M in sheared and unsheared thermally stratified flows with the initial density difference corresponding to $\Delta\overline{T}$ = 15 K: ○, $\Delta\overline{U}$ = 0 cm s^{-1}; ▽, $\Delta\overline{U}$ = 2 cm s^{-1}; ◇, $\Delta\overline{U}$ = 3 cm s^{-1}. (*b*) Streamwise distributions of the normalized salt flux versus x/M in sheared and unsheared salt stratified flows with the initial density difference corresponding to $\Delta\overline{T}$ = 15 K: ●, $\Delta\overline{U}$ = 0 cm s^{-1}; ▼, $\Delta\overline{U}$ = 2 cm s^{-1}; ◆, $\Delta\overline{U}$ = 3 cm s^{-1}.

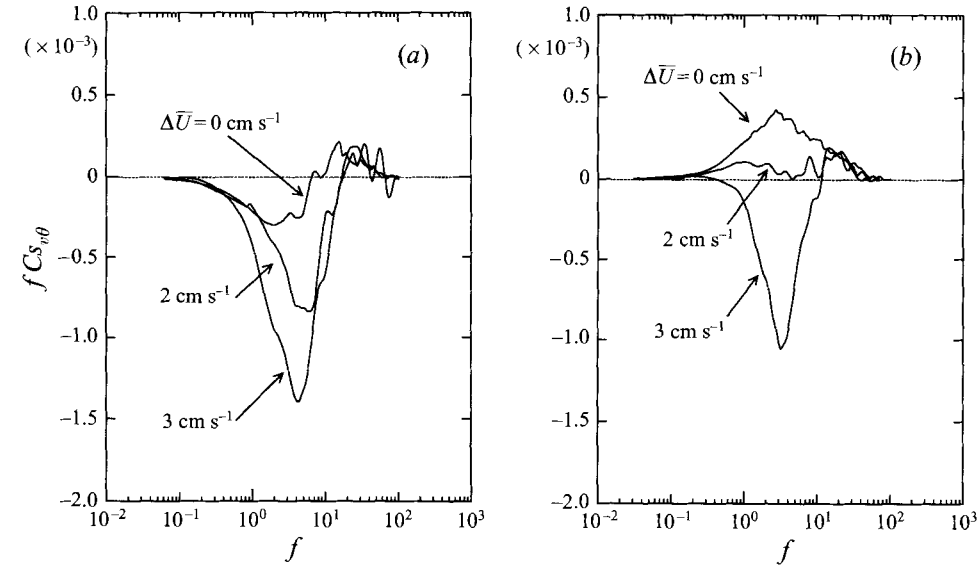

FIGURE 24. Cospectra of the vertical heat flux in the sheared thermally stratified flow with the initial temperature difference of $\Delta\overline{T}$ = 15 K; (*a*) at x/M = 10; (*b*) at x/M = 14. The cospectra are normalized by $\overline{U}\Delta\overline{T}$.

clear in salt stratification than in thermal stratification. For reference, the momentum, heat and salt fluxes are compared in the correlation coefficient form in figure 28. The correlation coefficients of the vertical heat and salt fluxes, $R_{v\theta}$ and R_{vc}, are close to those of the vertical momentum flux, R_{uv}, whereas the correlation coefficients of the longitudinal heat and salt fluxes, $R_{u\theta}$ and R_{uc}, are larger than $R_{v\theta}$, R_{vc} and R_{uv}.

To interpret the counter-gradient momentum transfer mechanism, the strongest salt-

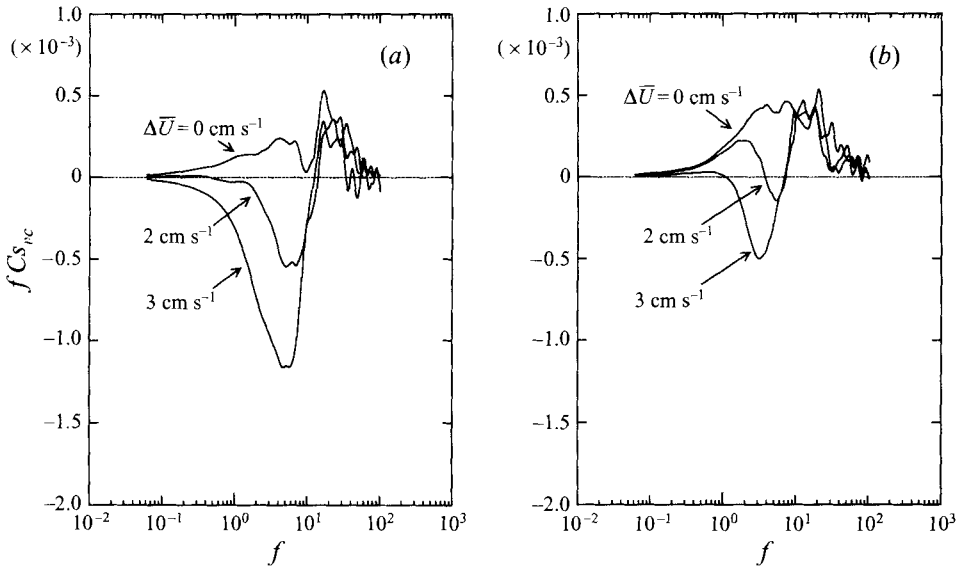

FIGURE 25. Cospectra of the vertical salt flux in the sheared salt-stratified flow with the initial density difference of $\Delta\overline{C}$ = 95 mol m^{-3}; (*a*) at x/M = 10; (*b*) at x/M = 14. The cospectra are normalized by $\overline{U}\Delta\overline{C}$.

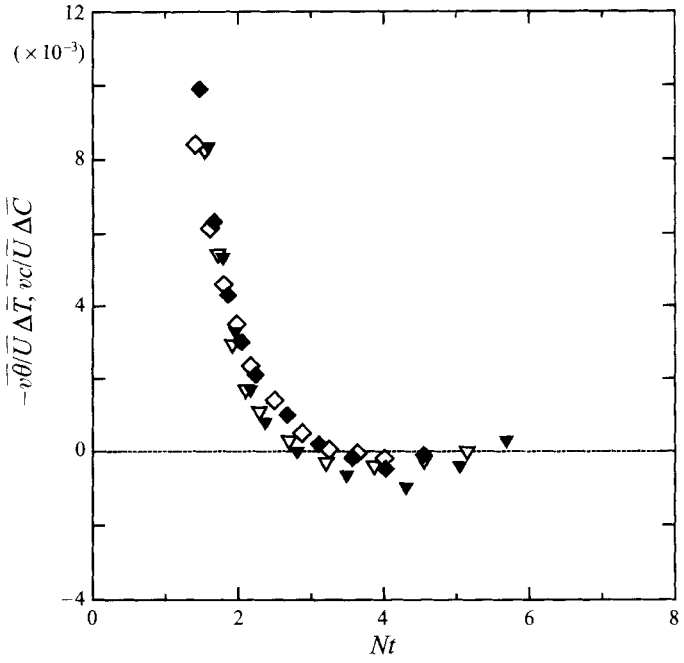

FIGURE 26. Streamwise distributions of the normalized heat and salt fluxes versus Nt in sheared density-stratified flows with the initial density difference corresponding to $\Delta\overline{T}$ = 15 K: ▽, thermal stratification with $\Delta\overline{U}$ = 2 cm s^{-1}; ◇, thermal stratification with $\Delta\overline{U}$ = 3 cm s^{-1}; ▼, salt stratification with $\Delta\overline{U}$ = 2 cm s^{-1}; ◆, salt stratification with $\Delta\overline{U}$ = 3 cm s^{-1}.

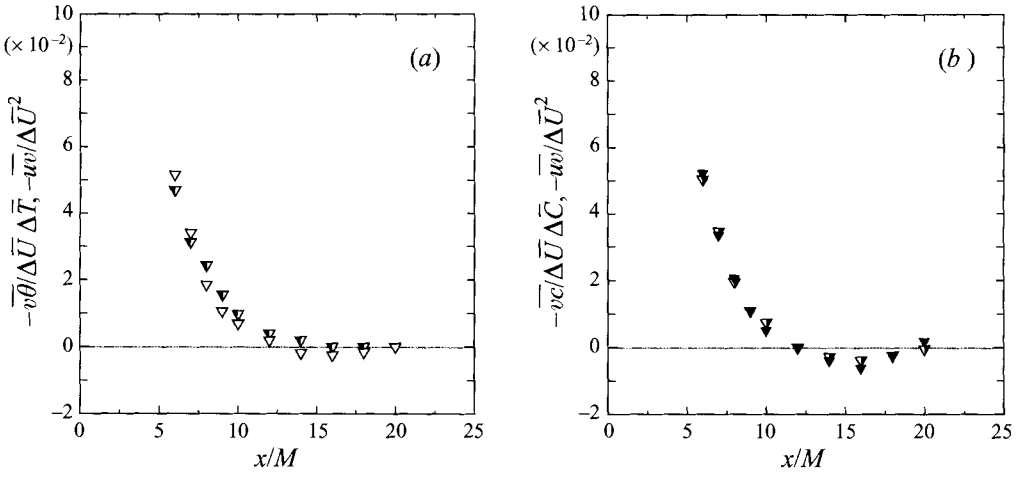

FIGURE 27. (*a*) Streamwise distributions of the normalized momentum and heat fluxes in the sheared thermally stratified flow with the initial velocity difference of $\Delta\overline{U} = 2$ cm s^{-1} and the initial temperature difference of $\Delta\overline{T} = 15$ K: ▼, $-\overline{uv}/\Delta\overline{U}^2$; ▽, $-\overline{v\theta}/\Delta\overline{U}\Delta\overline{T}$. (*b*) Streamwise distributions of the normalized momentum and salt fluxes in the sheared salt-stratified flow with the initial velocity difference of $\Delta\overline{U} = 2$ cm s^{-1} and the initial salinity difference of $\Delta\overline{C} = 95$ mol m^{-3}: ▼, $-\overline{uv}/\Delta\overline{U}^2$; ▼, $-\overline{vc}/\Delta\overline{U}\Delta\overline{C}$.

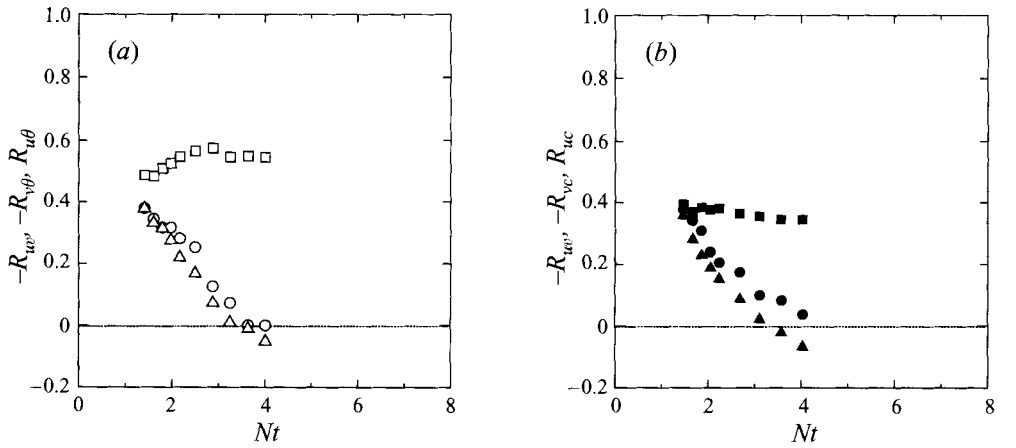

FIGURE 28. Distributions of the correlation coefficients versus Nt in sheared (*a*) thermally and (*b*) salt-stratified flows with the initial velocity difference of $\Delta\overline{U} = 3$ cm s^{-1} and the initial density difference corresponding to $\Delta\overline{T} = 15$ K: ○, $R_{uv} = \overline{uv}/u'v'$; △, $R_{v\theta} = \overline{v\theta}/v'\theta'$; □, $R_{u\theta} = \overline{u\theta}/u'\theta'$; ●, $R_{uv} = \overline{uv}/u'v'$; ▲, $R_{vc} = \overline{vc}/v'c'$; ■, $R_{uc} = \overline{uc}/u'c'$.

stratified flow with the initial density difference of $\Delta\overline{C} = 133$ mol m^{-3} corresponding to the temperature difference of $\Delta\overline{T} = 20$ K and the initial velocity difference of $\Delta\overline{U} = 2$ cm s^{-1} was analysed. The counter-gradient momentum and salt fluxes were clearly observed in the region $10 < x/M < 15$. Figure 29 shows the cospectra of u and v, Cs_{uv}, at $x/M = 6$, 10 and 14. When the cospectra Cs_{uv} are compared with the cospectra Cs_{vc} in the same flow (figure 30), it is found that for sheared stratified flows the counter-gradient momentum transfer mechanism is quite similar to the counter-gradient scalar transfer mechanism. That is, the counter-gradient momentum flux first

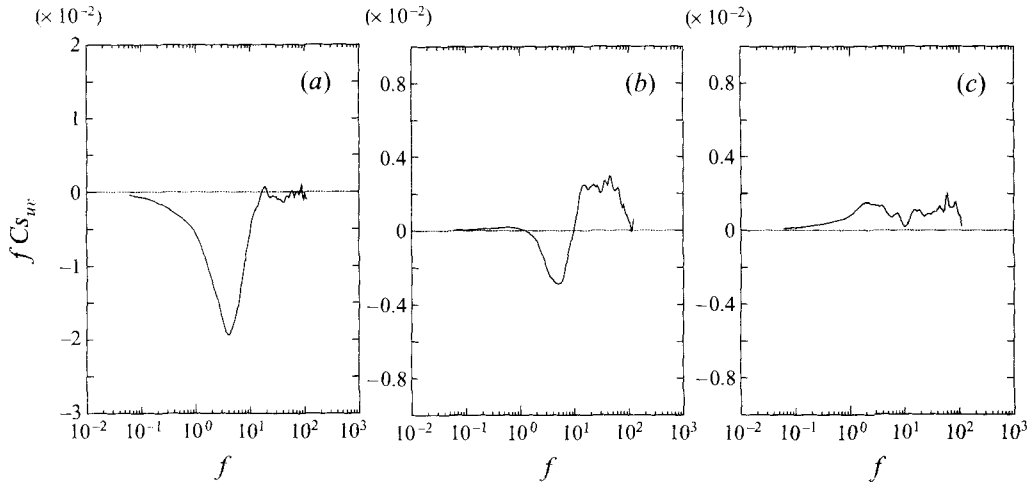

FIGURE 29. Cospectra of u and v in the sheared salt-stratified flow with the initial velocity difference of $\Delta\overline{U} = 2$ cm s^{-1} and the very large initial density difference of $\Delta\overline{C} = 133$ mol m^{-3}: (*a*) at $x/M = 6$; (*b*) at $x/M = 10$; (*c*) at $x/M = 14$. The cospectra are normalized by $\Delta\overline{U}^2$.

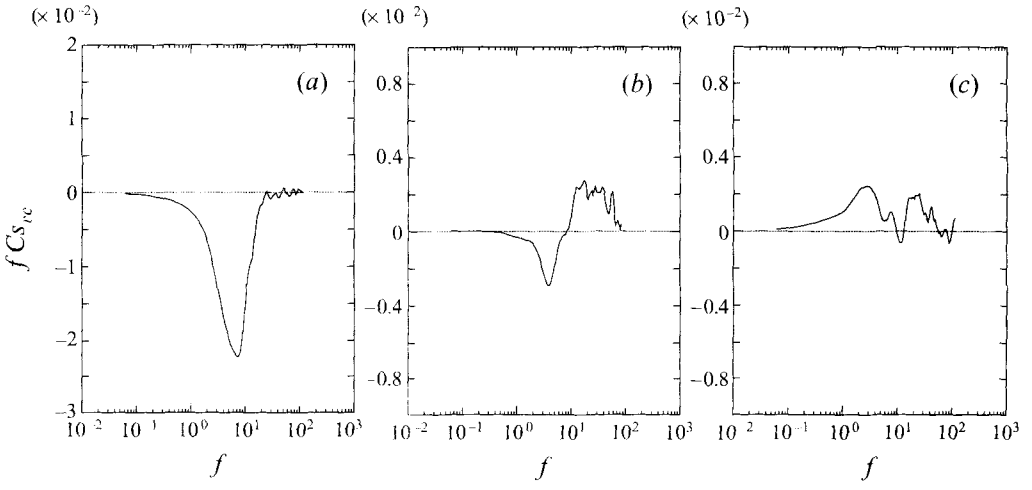

FIGURE 30. Cospectra of v and c in the sheared salt-stratified flow with the initial velocity difference of $\Delta\overline{U} = 2$ cm s^{-1} and the very large initial density difference of $\Delta\overline{C} = 133$ mol m^{-3}: (*a*) at $x/M = 6$; (*b*) at $x/M = 10$; (*c*) at $x/M = 14$. The cospectra are normalized by $\Delta\overline{U}\Delta\overline{C}$.

appears at small scales, and it prevails to large scales. The physical mechanism can easily be understood, if we consider buoyancy-driven small- and large-scale motions of the accelerated low-density fluid ($u > 0, \rho < 0$) and the decelerated high-density fluid ($u < 0, \rho > 0$) as well as the counter-gradient scalar transfer mechanism shown in figure 12. The momentum transfer mechanism has been qualitatively supported by LES of Kaltenbach *et al.* (1994) but the present results are different from the results of Rohr *et al.* (1988) which show little counter-gradient transfer at small scales. It should be particularly noted that in the measurements of Cs_{uv} by Rohr *et al.* (1988) the counter-gradient momentum transfer occurs at small scales in neutral stratification and the conceptual model of Gerz & Schumann (1996) also supports counter-gradient

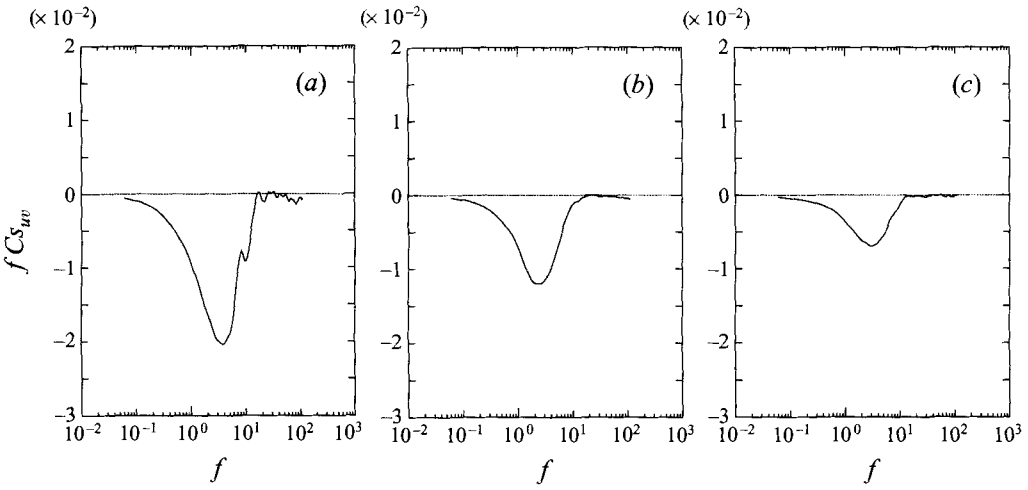

FIGURE 31. Cospectra of u and v in the sheared neutrally stratified flow with the initial velocity difference of $\Delta\overline{U} = 2$ cm s^{-1}: (*a*) at $x/M = 6$; (*b*) at $x/M = 10$; (*c*) at $x/M = 14$. The cospectra are normalized by $\Delta\overline{U}^2$.

transfer at small scales. However, the present measurements do not show any counter-gradient transfer at small scales in neutral stratification, as shown in figure 31. The difference may be due to the difference in the flow structure between homogeneous stratified flows (Rohr *et al.* 1988; Gerz & Schumann 1996) and the present stratified mixing-layer flows. However, linearized two-point correlation equations of Deissler (1961) have shown that down-gradient momentum transfer occurs at small scales in neutral stratification as well as in the present measurements. Of course, we should discuss whether the small-scale momentum transfer in neutral stratification can be described by a linear process (Gerz & Schumann 1996; Hanazaki & Hunt 1996). In the flow of Rohr *et al.* (1988) in an open channel with a low aspect ratio, the sign of the mean velocity gradient may slightly change due to the retardation effect of the free surface. Thus, it will be of interest to investigate more carefully whether the difference in the counter-gradient transfer mechanism at small scales in neutral stratification is caused by the difference between homogeneity and inhomogeneity.

3.3. *Difference in diffusion of active heat and passive mass*

Figure 32 shows the streamwise distributions of the normalized vertical fluxes of the active heat at $Pr \approx 6$ and the passive mass at $Sc \approx 600$ (sodium fluorescein dye) in unsheared strong thermal stratification. The difference between the fluxes clearly appears for $x/M > 8$ where counter-gradient transfer begins to occur. The counter-gradient flux of the passive mass is about 10 % larger than that of the active heat. The difference is more obvious in the counter-gradient fluxes in strong stratification than in the neutral case with large down-gradient fluxes, since the difference is attributed to the difference in the molecular diffusivities of the passive mass and active heat. Hunt (1985) has suggested a larger difference between active heat and passive mass, but the large difference between active and passive scalars is expected for different initial and boundary conditions as shown by Kaltenbach *et al.* (1994). The present thermally stratified flows have the same initial and boundary conditions for the active heat and the passive mass, i.e. the passive mass is well premixed in the high-temperature upstream (see figure 1). Therefore, the difference in the diffusion of the active heat

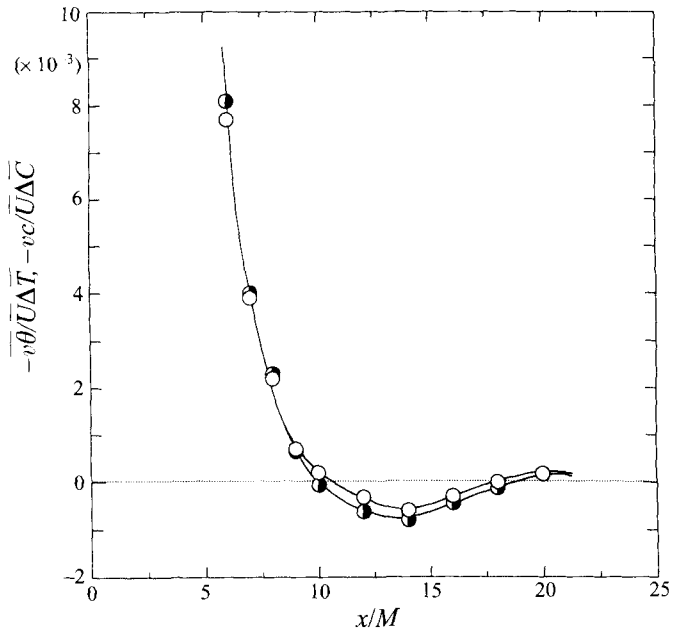

FIGURE 32. Streamwise distributions of the normalized vertical fluxes of the active heat and passive mass in the unsheared thermally stratified flow with $N_0 = 1.75\ \mathrm{s}^{-1}$: ○, $-\overline{v\theta}/\overline{U}\Delta\overline{T}$; ◑, $-\overline{vc}/\overline{U}\Delta\overline{C}$.

and the passive mass is small, and it occurs mainly at small scales as shown by the cospectra in figure 33(*a*). Figure 33(*b*) shows the coherence between the temperature fluctuation of the active heat and the concentration fluctuation of the passive mass at $x/M = 14$ in the same stratified flow. The coherence indicates that the correlation between the passive mass and the active heat rapidly decreases in the high-frequency region $f > 10\ \mathrm{s}^{-1}$. The rapid decrease of the correlation at small scales is generated by the large difference between the molecular diffusivities of the active heat and passive mass, since the present decaying turbulence is weak and suppressed by buoyancy in strong stratification. This can also be confirmed from the power spectra of the active heat and passive mass shown in figure 33(*c*). In addition to the difference in the magnitudes of two spectra, the cutoff frequency of the spectra clearly shows the effect of the molecular diffusivity. The influence of the molecular diffusivity is also significant in the scalar dissipation rates as shown in figure 34, and therefore the mean-squared temperature fluctuation decays more rapidly in the downstream region than the mean-squared concentration fluctuation as shown in figure 35.

4. Conclusions

The effects of molecular diffusivities and mean shear on counter-gradient scalar and momentum transfer were investigated in both sheared and unsheared density-stratified mixing-layer flows downstream of turbulence-generating grids. The main results from this study can be summarized as follows.

(i) The counter-gradient scalar and momentum transfer in stable stratification is strongly affected by the molecular diffusivity of the active scalar. For stratified water mixing-layer flows, the counter-gradient scalar and momentum fluxes are first observed at small scales, and then they spread to large scales. The counter-gradient

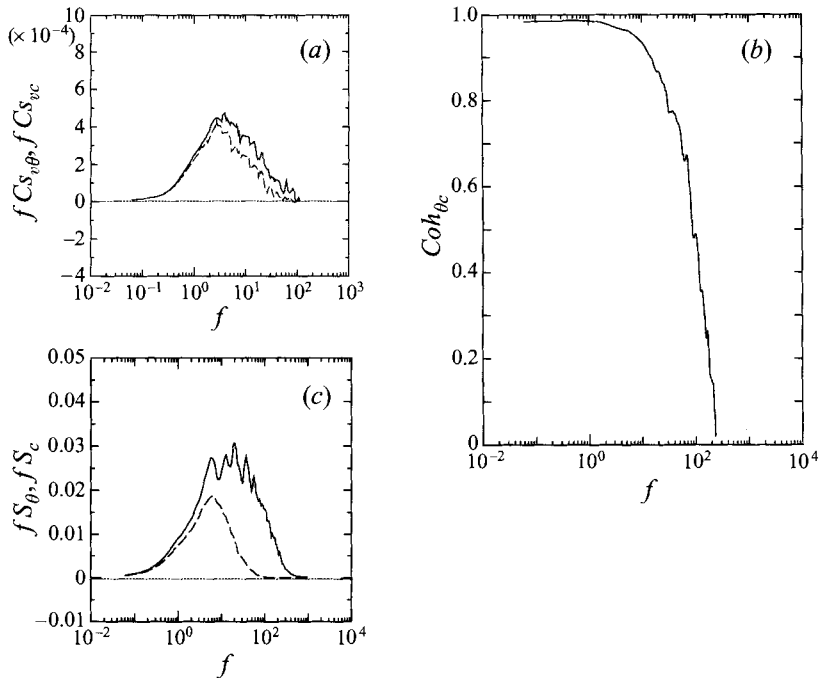

FIGURE 33. (*a*) Cospectra of the active heat and passive mass fluxes at $x/M = 14$ in the unsheared thermally stratified flow with $N_0 = 1.75\ \mathrm{s}^{-1}$: - - - - - - , $Cs_{v\theta}$; ——— , Cs_{vc}. The cospectra are normalized by $\overline{U}\Delta\overline{T}$ or $\overline{U}\Delta\overline{C}$. (*b*) Coherence between the temperature fluctuation of the active heat and the concentration fluctuation of the passive mass for the same flow as (*a*). (*c*) Power spectra of the temperature fluctuation of the active heat and the concentration fluctuation of the passive mass for the same flow as (*a*): - - - - - - , S_θ; ——— , S_c. The power spectra are normalized by $\overline{\theta^2}$ or $\overline{c^2}$.

fluxes are generated by buoyancy-induced motions and in particular finger-like motions are significant at small scales in stratified water flows. The counter-gradient scalar transfer mechanism is quite different for unsheared stratified water and air flows with different Prandtl or Schmidt numbers, since the small-scale motions in air flows more rapidly lose their available potential energy by molecular diffusion than the motions in water flows. Larger Prandtl or Schmidt numbers increase the buoyancy-oscillation period of the scalar fluxes. The time-oscillation of the counter-gradient scalar fluxes appears at large scales and the counter-gradient scalar fluxes at small scales persist without oscillating.

(ii) The mean shear acts to reduce counter-gradient scalar and momentum transfer in sheared stratified flows, but momentum transfer is generated by a similar mechanism to scalar transfer in unsheared stratified flows. In neutrally stratified mixing-layer flows, counter-gradient momentum transfer does not occur at small scales, which is in contrast to the previous studies of sheared homogeneous flows.

(iii) The difference in diffusion between active and passive scalars appears in strong thermal stratification. When the same initial and boundary conditions are applied to temperature and concentration fields, the counter-gradient flux of the passive mass becomes about 10% larger than that of the active heat. The difference is largest at small scales.

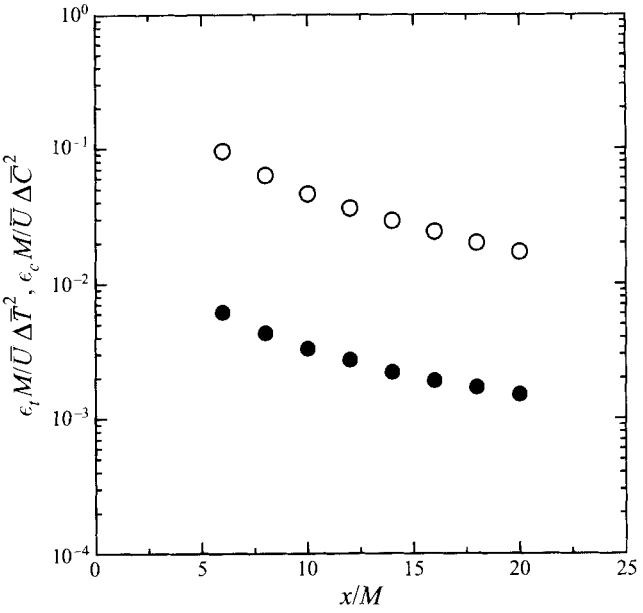

FIGURE 34. Streamwise distributions of the dissipation rates of active and passive scalars in the unsheared strongly thermally stratified flow with $N_0 = 1.75\ \mathrm{s}^{-1}$: ○, for temperature fluctuation; ●, for concentration fluctuation. The dissipation rates were roughly estimated by using an assumption of isotropic and frozen turbulence.

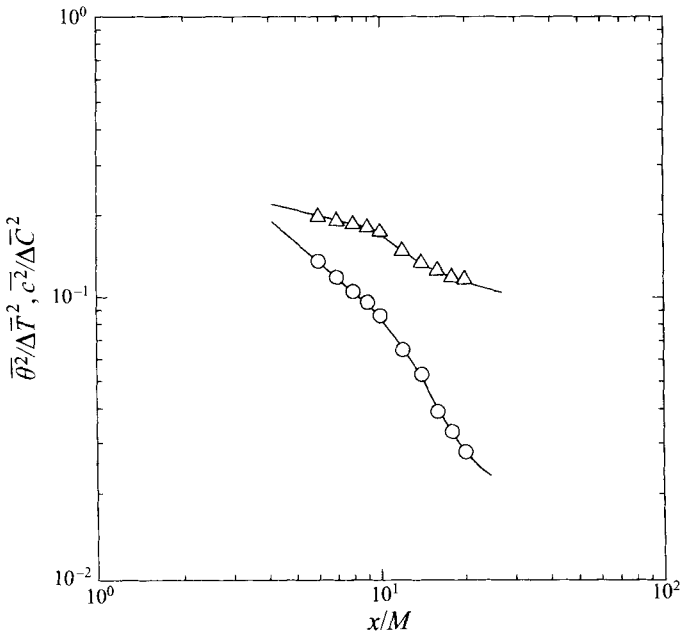

FIGURE 35. Streamwise variations of the mean-squared temperature and concentration fluctuations in the unsheared stratified flow with $N_0 = 1.75\ \mathrm{s}^{-1}$: ○, $\overline{\theta^2}/\Delta\overline{T}^2$; △, $\overline{c^2}/\Delta\overline{C}^2$

The authors would like to thank Messrs S. Okamura and H. Matsumoto for their help in conducting experiments. They are also grateful to three referees and Drs T. Gerz, J. C. R. Hunt and U. Schumann for their useful comments and Drs T. Kanzaki and H. Hanazaki for our discussions. This work was supported by the Japanese Ministry of Education, Science and Culture through grants-in-aid (No.07455087). The effects of the molecular diffusivities on the counter-gradient transfer were also discussed through the results of the direct numerical simulations carried out by using a super computer SX-3 of the Center for Global Environmental Research, National Institute for Environmental Studies, Environmental Agency of Japan.

REFERENCES

ANDRE, J. C., DE MOOR, G., LACARRERE, P., THERRY, G. & DU VACHAT, R. 1978 Modeling the 24-hour evolution of the mean and turbulent structures of the planetary boundary layer. *J. Atmos. Sci.* **35**, 1861–1883.

DEISSLER, R. G. 1961 Effects of inhomogeneity and of shear flow in weak turbulent fields. *Phys. Fluids* **4**, 1187–1198.

DEISSLER, R. G. 1962 Turbulence in the presence of a vertical body force and temperature gradient. *J. Geophys. Res.* **67**, 3049–3062.

FERNANDO, H. J. S. 1988 The growth of a turbulent patch in a stratified fluid. *J. Fluid Mech.* **190**, 55–70.

GERZ, T. & SCHUMANN, U. 1991 Direct simulation of homogeneous turbulence and gravity waves in sheared and unsheared stratified flows. In *Turbulent Shear Flows 7* (ed. F. Durst *et al.*), pp. 27–45. Springer.

GERZ, T. & SCHUMANN, U. 1996 A possible explanation of counter-gradient fluxes in homogeneous turbulence. *Theor. Comput. Fluid Dyn.* **8**, 169–181.

GERZ, T., SCHUMANN, U. & ELGHOBASHI, S. E. 1989 Direct numerical simulation of stratified homogeneous turbulent shear flows. *J. Fluid Mech.* **200**, 563–594.

GERZ, T. & YAMAZAKI, H. 1993 Direct numerical simulation of buoyancy-driven turbulence in stably stratified fluid. *J. Fluid Mech.* **249**, 415–440.

GIBSON, C. H. 1981 Fossil turbulence and internal waves. In *Nonlinear Properties of Internal Waves* (ed. B. J. West). AIP Conf. Proc. vol. 76, pp. 159–179.

GIBSON, M. M. & LAUNDER, B. E. 1978 Ground effects on pressure fluctuations in the atmospheric boundary layer. *J. Fluid Mech.* **86**, 491–511.

HANAZAKI, H. & HUNT, J. C. R. 1996 Linear processes in unsteady stably stratified turbulence. *J. Fluid Mech.* **318**, 303–337.

HANNOUN, I. A., FERNANDO, H. J. S. & LIST, E. J. 1988 Turbulence structure near a sharp density interface. *J. Fluid Mech.* **189**, 189–209.

HOLLIDAY, D. & MCINTYRE, M. E. 1981 On potential energy density in an incompressible, stratified fluid. *J. Fluid Mech.* **107**, 221–225.

HOLT, S. E., KOSEFF, J. R. & FERZIGER, J. H. 1992 A numerical study of the evolution and structure of homogeneous stably stratified sheared turbulence. *J. Fluid Mech.* **237**, 499–539.

HUNT, J. C. R. 1985 Diffusion in the stably stratified atmospheric boundary layer. *J. Climate Appl. Met.* **24**, 1187–1195.

HUNT, J. C. R., STRETCH, D. D. & BRITTER, R. E. 1988 Length scales in stably stratified turbulent flows and their use in turbulence models. In *Stably Stratified Flow and Dense Gas Dispersion* (ed. J. S. Puttock), pp. 285–321. Clarendon Press.

ITSWEIRE, E. C., HELLAND, K. N. & VAN ATTA, C. W. 1986 The evolution of grid-generated turbulence in a stably stratified fluid. *J. Fluid Mech.* **162**, 299–338.

JAYESH & WARHAFT, Z. 1994 Turbulent penetration of a thermally stratified interfacial layer in a wind tunnel. *J Fluid Mech.* **277**, 23–54.

JAYESH, YOON, K. & WARHAFT, Z. 1991 Turbulent mixing and transport in a thermally stratified interfacial layer in decaying grid turbulence. *Phys. Fluids* A **3**, 1143–1155.

KALTENBACH, H.-J., GERZ, T. & SCHUMANN, U. 1994 Large-eddy simulation of homogeneous turbulence and diffusion in stably stratified shear flow. *J. Fluid Mech.* **280**, 1–40.

KANZAKI, T. & ICHIKAWA, Y. 1995 Turbulence structure of a stably stratified grid-generated flow. In *Advances in Turbulence V* (ed. R. Benzi), pp. 266–270. Kluwer.

KOMORI, S. 1996 Turbulence structure and CO_2 transfer at the air-sea interface and turbulent diffusion in thermally-stratified flows. *CGER's Supercomputer Monograph Report*, vol. 1, *CGER-I021-'96*, Centre for Global Environmental Research, National Institute for Environmental Studies, Environment Agency of Japan.

KOMORI, S. 1980 Turbulence structure in stratified flow. PhD thesis, Dept. Chem. Engng, Kyoto University.

KOMORI, S., NAGATA, K., KANZAKI, T. & MURAKAMI, Y. 1993 Measurements of mass flux in a turbulent liquid flow with a chemical reaction. *AIChE J.* **39**, 1611–1620.

KOMORI, S., NAGATA, K. & MURAKAMI, Y. 1996 Heat and mass transfer in a stable thermally-stratified flow. *Dyn. Atmos. Oceans* **23**, 235–245.

KOMORI, S., UEDA, H., OGINO, F. & MIZUSHINA T. 1983 Turbulence structure in stably stratified open-channel flow. *J. Fluid Mech.* **130**, 13–26.

LIENHARD, V. & VAN ATTA, C. W. 1990 The decay of turbulence in thermally stratified flow. *J. Fluid Mech.* **210**, 57–112.

NAGATA, K. & KOMORI, S. 1996 Direct numerical simulation of the Prandtl number effect on the counter-gradient scalar transfer in strong stable stratification. *Trans. JSME* (in Japanese) (in press).

PEARSON, H. J., PUTTOCK, J. S. & HUNT, J. C. R. 1983 A statistical model of fluid-element motions and vertical diffusion in a homogeneous stratified turbulent flow. *J. Fluid Mech.* **129**, 219–249.

RILEY, J. J., METCALFE, R. W. & WEISSMAN, M. A. 1981 Direct numerical simulations of homogeneous turbulence in density-stratified fluids. In *Nonlinear Properties of Internal Waves* (ed. B. J. West). AIP Conf. Proc. vol. 76, pp. 79–112.

ROHR, J. J., ITSWEIRE, E. C., HELLAND, K. N. & VAN ATTA, C. W. 1988 Growth and decay of turbulence in a stably stratified shear flow. *J. Fluid Mech.* **195**, 77–111.

SCHUMANN, U. 1987 The countergradient heat flux in turbulent stratified flows. *Nucl. Engng Des.* **100**, 255–262.

STILLINGER, D. C., HELLAND, K. N. & VAN ATTA, C. W. 1983 Experiments on the transition of homogeneous turbulence to internal waves in a stratified fluid. *J. Fluid Mech.* **131**, 91–122.

YAMADA, T. & MELLOR, G. 1975 A simulation of the Wangara atmospheric boundary layer data. *J. Atmos. Sci.* **32**, 2309–2329.

YOON, K. & WARHAFT, Z. 1990 The evolution of grid-generated turbulence under conditions of stable thermal stratification. *J. Fluid Mech.* **215**, 601–638.